Polymer 51 (2010) 4639–4662

Contents lists available at ScienceDirect

Polymer

journal homepage: www.elsevier.com/locate/polymer

Feature Article

Mesophases in polyethylene, polypropylene, and poly(1-butene)

René Androsch [a], Maria Laura Di Lorenzo [b], Christoph Schick [c], Bernhard Wunderlich [d,e,*,1]

[a] Martin-Luther-University Halle-Wittenberg, Center of Engineering Sciences, D-06099 Halle/S., Germany
[b] Istituto di Chimica e Tecnologia dei Polimeri (CNR), c/o Comprensorio Olivetti, Via Campi Flegrei 34, 80078 Pozzuoli (NA), Italy
[c] University of Rostock, Institute of Physics, Wismarsche Straße 43-45, D-18051 Rostock, Germany
[d] Department of Chemistry, University of Tennessee, Knoxville, USA
[e] Chemical Sciences Division, Oak Ridge National Laboratory, Oak Ridge, TN, USA

ARTICLE INFO

Article history:
Received 15 April 2010
Received in revised form
14 July 2010
Accepted 17 July 2010
Available online 4 August 2010

Keywords:
Equilibrium
Mesophase
Metastability
Molecular motion
Phase transition
Poly(1-butene)
Polyethylene
Polypropylene
Structure
Thermodynamics

ABSTRACT

This paper contains new views about the amorphous and partially ordered phases of the three polymers listed in the title. The discussion is based on information on structure, thermodynamic stability, and large-amplitude molecular motion. Polyethylene is the basic backbone of all alkene polymers, and the other two are the first members of the vinyl polymers which have stereospecifically placed alkyl side chains. Their multiphase structures consist of metastable crystals, mesophases, and surrounding rigid and mobile amorphous fractions. All these phases have sizes ranging from micrometer dimensions down to nanometers. Besides the phase structures, information about the molecular coupling between the phases must be considered. Depending on temperature, the polymer phases can vary from solid (rigid) to liquid (mobile). New knowledge is also gained by cross-comparison of the title polymers. The experimental information was gained from (a) various forms of slow, fast, and temperature-modulated thermal analysis to identify equilibrium and non-equilibrium states, (b) measurement of structure and morphology at various length scales, and (c) tracing of the large-amplitude molecular motion, the kinetics of order/disorder changes, and the liquid/solid transitions (glass transitions). It is shown that much more needs to be known about the various phases and their coupling to characterize a given polymer and to fine-tune its properties for a given application.

1. Introduction

1.1. The multiphase structure

semi-crystalline polymers have a metastable, multiphase structure with superstructures of dimensions from macroscopic (above 1 μm) to nanometers. The common morphologies vary in character from lamellar (as single lamellae, hedrites, spherulites, or dendrites) to fibrillar or nodular, detected by optical, electron, or atomic force microscopy. The crystals are in most cases much smaller than the molecules are long. This forces the molecules either to fold (chain-folding principle [1, Sect. 3.2.2.1]), or to assume a fringed micellar macroconformation which couples multiple phases [1, Fig. III.5].

To understand such complicated systems, it is of importance to know the crystal structures and the molecular motion. The crystal structure is usually derived from diffraction experiments. To directly assess molecular motion, one can use infrared spectroscopy (IR), Raman spectroscopy, or solid state nuclear-magnetic resonance (NMR). With macroscopic calorimetry one can judge thermal motion by interpretation of the heat capacity, $C_p = (\partial H/\partial T)_{p,n}$, which represents the change in enthalpy, H, with temperature, T, at constant pressure, p, and composition, n [2]. Critically reviewed experimental values of C_p are collected in the ATHAS Data Bank [3]. From calorimetry, one can also assess the degree of order via the latent heat, L, by evaluation of entropy changes, ΔS, during equilibrium transitions. A full thermodynamic description must consider the global, usually non-equilibrium nature of the sample and separate contributions from the local subsystems or phases. Errors due to changes during measurement at time scales similar to those innate to the unstable components must be avoided [2].

The crystals are surrounded by amorphous phases which can be characterized by their glass transition. Above the glass transition temperature, T_g, the amorphous material is considered to be mobile (mobile amorphous phase, MAF). The glass transition is usually broadened to higher temperature from that of the entirely amorphous phase, the bulk-amorphous phase. Amorphous domains

* Corresponding author at: Department of Chemistry, University of Tennessee, Knoxville, USA. Tel.: +1 855 675 4532.
E-mail address: Wunderlich@CharterTN.net (B. Wunderlich).
[1] Present address: 200 Baltusrol Road, Knoxville, TN 37934-3707, USA.

0032-3861 Published by Elsevier Ltd. Open access under CC BY-NC-ND license.
doi:10.1016/j.polymer.2010.07.033

bordering the crystals may remain solid up to a separate, higher T_g and are called a rigid-amorphous fractions, RAF, [2]. Earlier, the RAF was called an 'amorphous crystal-defect' because of its close coupling to the crystal [1, vol. 1]. Above its T_g, C_p of the RAF is similar to that of the liquid MAF as it is extrapolated from the melt data.

1.2. The different molecular motions

The relaxed, amorphous liquid of flexible, linear macromolecules (also designated as melt) can be considered to be in thermodynamic equilibrium. On lowering of the temperature, the glassy, solid state is approached due to slowing of the cooperative, large-amplitude motion. Depending on the molecular structure, this large-amplitude motion can consist of intramolecular conformational motion and for small molecules also of rotation and translation of the whole molecule. Relative to the liquid, the glass represents a metastable state with practically all of its heat capacity generated by vibrations (small-amplitude motions). The amorphous structure and enthalpy of liquid and glass are identical when extrapolated to their T_g, resulting in zero entropy change, ΔS, and a non-zero change in heat capacity, ΔC_p.

The small-amplitude thermal motion in the glassy and crystalline solid states can be separated into group vibrations and skeletal vibrations, as is indicated in Fig. 1 for PE crystals. The group vibrations are usually of high frequency (10–100 THz), and for the same chemical structure, they are largely independent of the degree of disorder, i.e., are similar in glasses and crystals. The skeletal vibrations, in turn, reach from the acoustical frequencies to about 10 THz. The contributions of the large-amplitude motion and the skeletal and group vibrations to C_p are known for many polymers from thermal analysis, while the contributions from the group vibrations can also be calculated from their infrared and Raman spectra [4].

1.3. The different phases

For molecules of a sufficiently regular chemical structure, lowering of the temperature of a liquid may introduce different degrees of order by crystallization [1] or mesophase formation [5]. Any phase with sufficient cooperative, large-amplitude mobility will undergo a glass transition on cooling [6]. Comparing different phases of the same chemical composition at a given T, the most stable phase has the lowest free enthalpy, G (Gibbs energy, $G = H - TS$).

To assess the energetics of phases of linear, flexible macromolecules, one first establishes the intramolecular bond energies between the atoms. A second, lesser contribution comes from the conformational energy due to internal rotation and its corresponding intramolecular steric hindrance. This is followed by the packing of the molecules of given conformation by considering intermolecular van der Waals interactions, and for more polar molecules, other weak bonding, such as dipole interaction and hydrogen bonding [1, Sect. 2.3]. The fourth contribution comes from the vibrational spectrum, as given for PE in Fig. 1. To the vibrational contributions those from large-amplitude molecular motion are to be added.

Fig. 2 presents a schematic of the ten possible phase types [1,5,6] as distinguished by their glass and disordering transitions. This scheme developed over the years, as documented by the publications [1,5,6]. The glass transitions, marked on the left side of the figure, link mobile and solid condensed phases of the same structure. The glass transitions are time-dependent and occur over a temperature range centered at T_g, the temperature of half-completion of the ΔC_p.

The disordering transitions on the right, in contrast, may be sharp and reversible. The schematic also lists the connections to the possible transition entropies on disordering. The overall entropy increase on fusion, $\Delta S_{(fusion)}$, refers to the equilibrium transitions from crystal to melt (liquid). The three mesophase crystals are increasingly disordered when going from top to bottom. Plastic and liquid crystals are not connected by disordering transitions because of their incompatible structure requirements (mesogen shapes) [5, Sect. 2]. The five upper phases are solid phases, with even some crystals, such as poly(oxyethylene) and aliphatic nylons, being solid only below the T_g of their crystals occurring separate from the melting temperature, T_m [6].

The flexible, linear macromolecules can be characterized by four overall shapes or macroconformations [1, Fig. III.5]: The 'folded-chain' and the 'fringed micellar' macroconformations are usually metastable. All spontaneous ordering from the third macroconformation, the 'random coil,' found in the liquids, yields more stable states, but rarely equilibrium. The 'extended-chain' macroconformation is found in equilibrium crystals. It may develop on

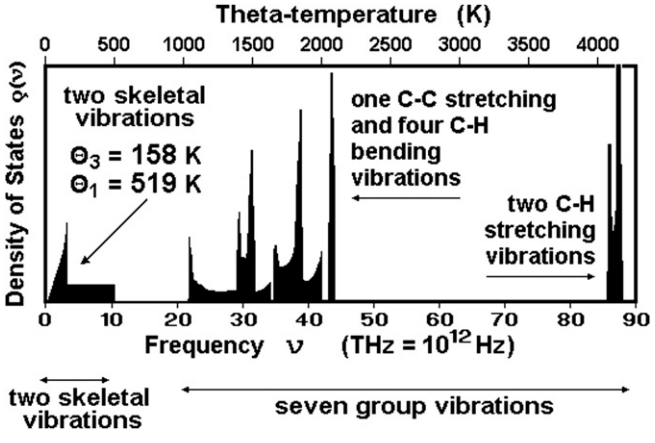

Fig. 1. Approximate vibrational spectrum of crystalline PE which reproduces the C_p from 0 K to the beginning of large-amplitude motion. Glassy PE shows the same spectrum except for a change of Θ_3 to 80 K ($\Theta = h\nu/k$ where h and k are the Planck and Boltzmann constant, respectively). The theta temperatures Θ_3 and Θ_1 designate the limiting three-dimensional and one-dimensional Debye temperatures, respectively [2,4].

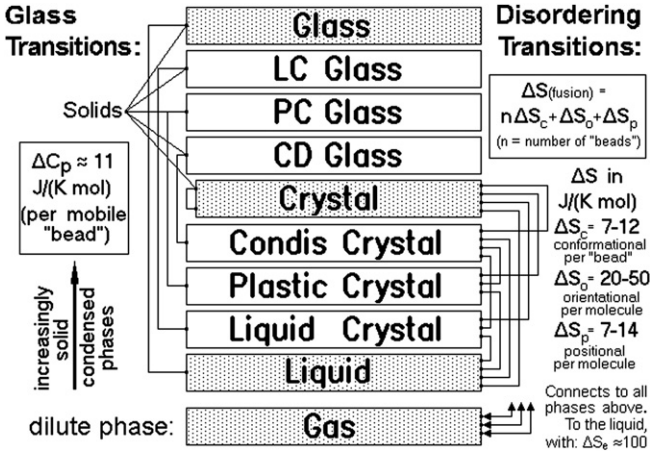

Fig. 2. A schematic of the 10 types of phases and their typical transitions. Also marked on the left are the mechanical appearances and heat capacity changes, ΔC_p, at T_g. On the right the approximate increases in entropy, ΔS, are listed on disordering as caused by the various large-amplitude motions. The 'bead' corresponds to the molecule or part of the molecule undergoing large-amplitude motion. The progression of the phases from top to bottom commonly involves an increase in T.

annealing of mesophases with sufficient chain mobility or by direct crystallization from the monomer to the polymer crystal (crystallization during polymerization) [7].

Since in semi-crystalline samples the macromolecules may bridge several phases, they are coupled across their phase boundaries. This coupling may influence the phase transitions [8], and ultimately may create additional phases, such as the RAF, which was first described in [9].

1.4. The different polymers

The industrially most important linear polymer is polyethylene (PE) with a monomer-based repeating unit of CH_2–CH_2–. In addition to molar mass, polydispersity, and thermal as well as mechanical history, the properties of PE and other polymers, are influenced by the chemical microstructure. The common types of PE with different microstructure are:

1. Polymethylene (PM), also the structure-based name of PE. It has a strictly linear structure (LPE), $(CH_2-)_x$. It was first made by decomposition of diazomethane [10] and named long before flexible macromolecules were recognized as a special class of molecules.

2–5. Low-density PE (LDPE), was the first industrial PE. It was developed in the 1930s [11], synthesized from ethylene, CH_2=CH_2, at high pressure via free-radical processes. It contains many statistically placed paraffinic branches of four and five carbon atoms, in addition to some long branches. Both of these structure defects reduce the maximum crystallinity that can be reached by cooling a melt of LDPE. Later, other low-density variations of PE were introduced and characterized as: Linear-low-, Very-low-, or Ultra-low-density PE (LLDPE, VLDPE, and ULDPE, respectively).

6–7. High-density polyethylene (HDPE) is predominantly linear. It was developed by the 1950s, using syntheses at low-pressure [12,13]. Industrially, HDPE contains a small number of branches, deliberately introduced by copolymerization or from intrinsic side-reactions of the synthesis. A distinct variety of such linear polyethylene, Ultra-high Molar Mass PE (UHMMPE) has been developed predominantly as material for high-strength PE fibers.

The thermal properties of most of the different PEs are summarized in [14]. The shape of lowest energy of a PE molecule is a planar zigzag with all C–C-bonds in a trans-conformation, shown as the left entry in Fig. 3 for a 12 repeating unit sequence. Metallocene, single-site catalysts were discovered in 1976 [15]. They allow not only tailor-making polyethylenes (mPE), but are used mainly to synthesize copolymers of fixed microstructure within and between molecules.

Propylene, CH_2=$CH(CH_3)$, is the second in the series of alkenes. Its methyl group characterizes the double-bond of the monomer as a vinyl group. The repeating unit of polypropylene (PP), thus, is CH_2–$CH(CH_3)$–. Using free-radical polymerization, as for the

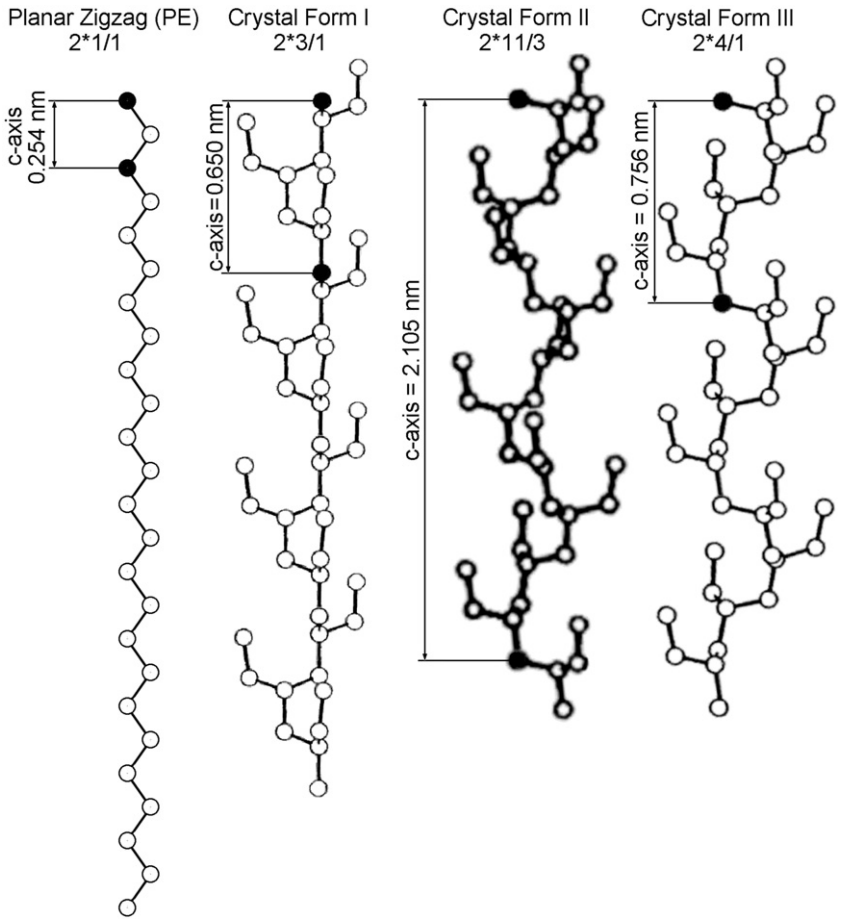

Fig. 3. The four helix types of PE, iPP, and iPB. The planar zigzag is illustrated for PE. It is found in all its polymorphs. The polymorphs of iPP show the same helix type as the illustrated crystal form I of iPB. To appreciate the decrease in the overall length of the helices, every segment is drawn for 12 molecular repeating units. The crystal *c*-axis lengths of the planar zigzag corresponds to the orthorhombic PE, the monoclinic iPP has the same *c*-axis length as iPB (see also Fig. 11, below).

synthesis of LDPE, however, yields an atactic polymer (aPP). In aPP the methyl groups are randomly placed above or below the planar zigzag shown for PE in Fig. 3. Such aPP cannot crystallize and remains rubbery down to its T_g. In isotactic polypropylene (iPP), to be discussed in this paper, all methyl groups are placed on the same side of the planar zigzag of Fig. 3.

Industrially useful, highly isotactic PP could only be produced after the iPP synthesis was discovered in the 1950s using Ziegler–Natta catalysts [16]. The invention of the synthesis of iPP [17] was, however, made in a number of different laboratories within a very short time period, so that it took some 30 years and many law suits until a legal resolution of the patent was established in 1983 [18,19]. By this time, iPP was already one of the most produced plastics.

Isotactic poly(1-butene) (iPB), finally, has the repeating unit CH_2–$CH(C_2H_5)$–. It has ≈50% of all its matter located in the short side chains and is a thermoplastic vinyl polymer with outstanding mechanical properties and resistance to many solvents. Despite the excellent properties, the applications of iPB are limited due to its more complex polymorphism when compared to PE and iPP. The iPB can develop five crystal modifications with a variety of helix conformations when subjected to different thermal and mechanical histories [20–23]. The three most important modifications are displayed in Fig. 3 as crystal forms I–III, drawn after Ref. [22].

The intramolecular steric hindrance between the methyl groups of iPP and ethyl groups of iPB forces the backbone into the helical structures shown in Fig. 3. The helices of the crystal form I of iPB may be right-handed or left-handed with regular gauche-trans sequences of the C–C-backbone. Tracing the iPB helices in Fig. 3 from the bottom to the top, one finds that the rotations are counterclockwise, making the helices left-handed. In addition, the ethyl groups are not normal to the axis of the helix, but inclined. In Fig. 3, they all point 'up'. A helix may, thus, be placed in four ways onto a crystal surface, as a left-handed or right-handed helix, and one of two inclinations of the methyl groups, all 'up' or all 'down' [1, Fig. II.28].

In Fig. 3 all molecules are drawn as sequences of 12 repeating units in order to compare the shortening of the different helixes. The iPP conformation is identical to that found in form I of iPB, but with methyl groups instead of the ethyl groups. All three polymers are of 'class 2', i.e., they have repeating units of two backbone atoms. (But note, if considering PE as PM, it is of 'class 1' with a repeating unit of CH_2–.) The class 2 helix of iPP with its two backbone atoms completes after every third monomer one turn of the helix. Following this description, the helix point-net notation designates it as 2*3/1. The 2*3/1 helix is the basic, low-energy conformation in all polymorphs of iPP, but the helix symmetry is not part of the symmetry of the crystals.

This just defined helix point-net notation is different from the screw axis notation of crystal symmetry and is preferred to describe helical molecules. The crystal screw axis does not necessarily generate consecutive repeating units of the helices on the crystal lattice. A right-handed 2*3/1 helix can be described by a 3_1 crystallographic screw axis, but a left-handed 2*3/1 helix, as drawn in Fig. 3, is not equivalent to a 3_2 crystallographic screw axis since only right-handed rotations are used in the description of crystal symmetries. A 3_2 screw axis (producing 1/3 of a right-handed turn and a $2c/3$ translation) yields the proper symmetry, but repeats itself only after two unit cell lengths, i.e., it does not follow the structure of the molecule, rather, it needs an added c-translation to fill-in the parts of the molecule missed by the $2c/3$ translation. Together, the right-handed 1/3 turn, $2c/3$ translation forward, followed by a c-translation backwards, produces the left-handed 2*3/1 helix.

Continuing the isotactic alkene polymer series, it becomes increasingly difficult to combine a backbone with a linear paraffinic side chain to a perfect crystal. Ultimately, the crystals assume the character of paraffins of double the length of the side group accommodating the backbone in the middle. In line with these changes in crystal structure, the T_m of the isotactic alkene polymers decreases from a high for iPP (461 K) to reach a minimum of about 300 K in the range from poly(1-hexene) to poly(1-nonene) [1, Tables VIII.4 and X.10]. This low T_m is close to that of octadecane ($C_{18}H_{38}$) of 297 K. Thereafter, T_m increases again and reaches 365 K for poly(1-docosene), to be compared to 360 K for tetratetracontane ($C_{44}H_{90}$). Finally, it should reach the T_m of PE of 414.6 K.

The alkene polymers with low T_ms are difficult to crystallize [1,24] because of their two opposing structure elements. As the side chain becomes longer, the backbone chain is increasingly decoupled from the main crystal elements and acts as a defect, negating also the need of stereospecificity for crystallization. These polymers with long paraffin side chains can also use different backbone chains for similar crystal structures. An example of a study of the latter is that of poly(octadecyl acrylate) (PODA) with a repeating unit of CH_2–$CH(COO\{-CH_2\}_{17}-CH_3)$–. Its paraffinic side chains contain ≈80% of the molecular mass. As expected, PODA has a T_m of ≈320 K [25], not far from that of octadecane, and it has lost the double layer nature of the isotactic polyalkenes with shorter side-chain lengths [1, Sect. 10.3.4]. Similar decoupling is possible for precisely synthesized long-chain methylene sequences which are regularly interrupted by different structure elements. For example, PE with side groups placed at every 21st methylene of the backbone by attaching methyl, ethyl, or two methyl groups were studied in detail (PE1 M, T_m ≈ 338 K; PE1E T_m ≈ 309 K; and PE2 M T_m ≈ 320 K, respectively) [25]. It is interesting to note that despite the paraffin-like T_ms, the crystal morphology of these molecules remains that of a macromolecule with lamellar, chain-folded crystals of similar fold lengths as found for PE. The decoupled non-fitting groups are located on defect planes within the overall crystal [25,26].

In this paper, the three title polymers are to be compared and discussed within the framework of their molecular motion and thermodynamics as it fits into the schematic of the phase types and properties displayed in Fig. 2 and the molecular conformations summarized in Fig. 3. As expected, all mesophases to be discussed are conformationally disordered (condis crystals or CD glasses) [5]. The main types of phases of Fig. 2 used in the comparison of the title polymers are liquids, condis crystals, crystals, CD glasses, and glasses. The CD glasses (condis crystals cooled below their T_g), as well as the various forms of amorphous glasses have frozen chain conformations and are not able to change their order below T_g. Since these glass transitions are frequently rather broad, it is important to know their full temperature range. For example, low temperature crystallization of PE can occur below T_g, but still within its glass transition range which reaches to lower temperatures than the value defined in Sect 1.3 as T_g, as will be described in Sect. 2.5, below. The needed data of C_p of the liquid and solid phases for all three polymers can be found in [27] and the ATHAS Data Bank [3].

2. The phases of polyethylene (PE)

2.1. Polymorphism and molecular mobility of PE crystals

The low-energy, planar zigzag chains of PE as given in Fig. 3 can be considered to be a degenerate helix of type 2*1/1, i.e., it is generated by a turn of 360° per $(CH_2-)_2$. For the identical PM molecule, the planar zigzag can be considered a 1*2/1 helix with a turn of 180° per CH_2–. One finds two possible close-packed crystal structures for PE [28]. In one, the planes of the zigzag chains

are parallel with triclinic or monoclinic symmetry, the other is orthorhombic with two chains per unit cell with the planes rotated ≈90° [1, Figs. II.34–36]. In both structures, every PE chain has a coordination number of six for nearest neighbor chains [1, Sect. 2.3.6].

Orthorhombic crystals are found on crystallization of PE by cooling from the quiescent melt or solution. This is also the crystal structure for the longer straight-chain paraffins. First detailed X-ray experiments for PE were made by Bunn [29]. He assigned the unit cell to the (non-standard) setting P*nam* which places the chain direction parallel to the crystallographic *c*-axis. (The standard setting would be P*nma* [1, Sect. 2.2.4]). The twofold screw axis, 2_1, two centers of symmetry, *i* (at the centers of the C–C-bonds), and the mirror plane, *m*, through the methylene groups of the molecule are also part of the crystal symmetry.

The second polymorph was identified in drawn PE by Turner-Jones [30] as being closely related to the triclinic crystal structures of the *n* paraffins shorter than docosane. In contrast to the paraffins, polyethylene, however, retains a mirror plane (*m*) parallel to the chain direction, doubling the unit cell to two chains and increasing the crystal symmetry to monoclinic, C2/*m* [1,31] which places the chain direction along the crystallographic *b*-axis.

The complete vibrational spectrum of orthorhombic PE was assembled from the analysis of the low temperature C_p for the approximation of the skeletal vibrations [27,32], while the group vibrations were gained from normal mode calculations based on IR and Raman spectroscopy [33]. Fig. 1 shows the vibrational spectrum which agrees up to room temperature with the C_p measured for equilibrium crystals of PE [34]. For the monoclinic polymorph, one expects only an insignificant decrease in Θ_3 from the value listed in Fig. 1.

2.2. The condis crystals of PE and paraffins

The crystal structure of the mesophase of PE was discovered by Bassett [35] as a high pressure phase with hexagonal packing of the chains. Before this discovery, it was already shown that crystallization under elevated pressure [36,37] must lead to higher chain mobility in the crystals to yield extended-chain crystals from the initially-grown, chain-folded macroconformation which is required by the chain-folding principle, mentioned in Sect. 1.1.

Fig. 4 illustrates the drastic change of the crystal structure with temperature at elevated pressure [38]. In the schematic of Fig. 2, the mesophase of PE is a condis crystal [5]. The disordering transition to the condis phase is characterized by a ΔS of more than half of the entropy of fusion of the orthorhombic crystal [39, Sect 4.1]. This high entropy resolves the puzzle that higher pressure can favor a mesophase structure for the PE chain. The higher temperature allows to populate mobile conformational defects. In the time it takes to determine the X-ray structure, the defect chains are averaged to symmetric cylinders which are interpenetrated at any instant by the neighboring chains. This actual motion in a condis crystal could be simulated by molecular dynamics calculations [40]. The averaging allows the chains to occupy a position of hexagonal symmetry in the crystal despite their lower molecular symmetry. The volume-increase on going to the condis phase is less than expected by rotation of the zigzag plane as a whole, and its entropy gain is considerably higher since each rotating segment gains the entropy of a 'bead', as listed in Fig. 2. Fig. 5 represents the phase diagram of PE, as discussed in [1, Sect 8.5.2]. The increasing range of stability of the condis phase with temperature and pressure is linked to the smaller increase in disorder on isotropization than on the initial disordering from the crystal [39, Sect. 4.1].

A condis phase for *n* paraffins with 9–44 chain atoms with chain disorder and hexagonal symmetry is also observed, but at atmospheric pressure. This mesophase was first described as a 'rotor phase', implying the rotation of the whole planar zigzag [41]. Its entropy of disordering from the crystal, however, is bigger than for typical solid–solid transitions and smaller than the orthorhombic to condis phase transition of PE. Still, it is larger than can be estimated from Fig. 2 for the orientational disordering of the whole molecule. From docosane to hexatriacontane, ΔS_c per mole of rotatable C_2H_4– is practically constant at 6.8 J K^{-1}, while

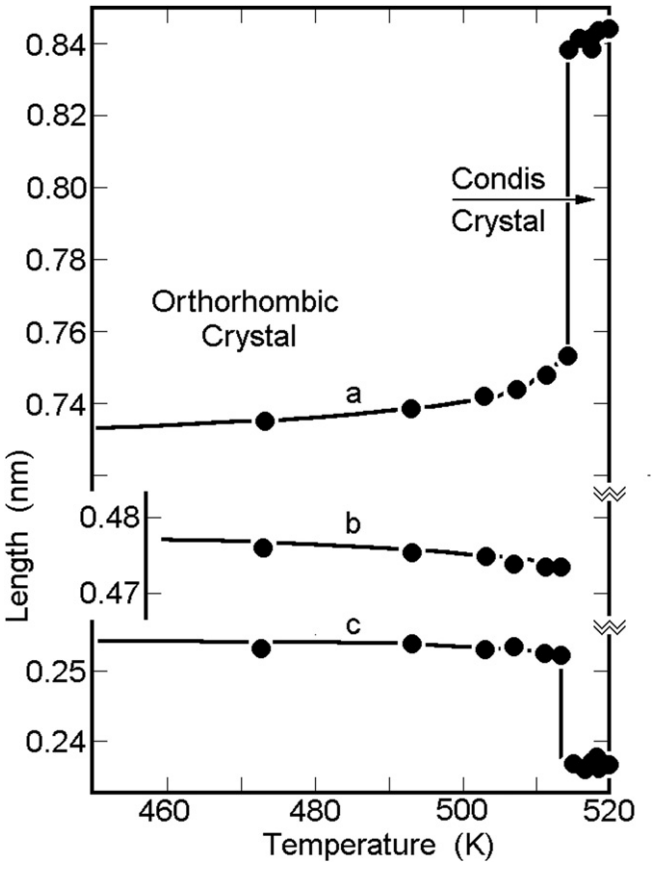

Fig. 4. Change of lattice parameters of polyethylene at 500 MPa pressure measured by X-ray diffraction [38]. The *a*-spacing of the condis crystal is multiplied with 2×cos 30° to permit a direct comparison with the orthorhombic *a*-spacing.

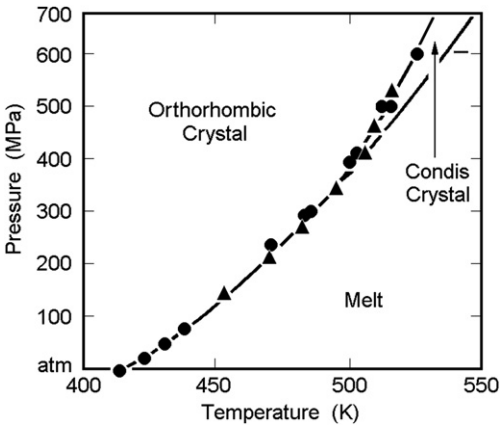

Fig. 5. Phase diagram of polyethylene as discussed in [39, Sect. 4.1] The condis-melt boundary has a shallower slope due to its lower entropy of disordering than measured for the orthorhombic-condis crystal transition.

according to Fig. 2, as a molecular rotator, ΔS_o for the whole molecule should decrease from about 4.0 to 2.0 $J K^{-1}$ (mol of $C_2H_4)^{-1}$ [42]. Also, the activation energy for rotation of the whole chain would be rather high since the volume-increase is insufficient for a free rotation. Because the entropy of isotropization of the condis phase of the paraffins is larger than the disordering on going from crystal to condis crystal, in contrast to PE, the phase area of stable condis phases of paraffins decreases with increasing pressure. Below molar mass of 6500 Da no condis crystals were observed for PE at high pressure [43].

From the thermodynamic data, it was concluded that the mesophases of PE and *n* paraffins are not liquid crystals. Estimates for ΔS_p of liquid crystals, as given in Fig. 2, would require a much lower isotropization entropy than is found for the typical condis crystal [5,39].

In the condis phase, the process of chain extension is accelerated. Although not all condis crystals known for different flexible macromolecules anneal to extended-chain crystals, all known extended-chain crystals have seen an intermediate condis phase when grown from the random coil of the melt or solution. A direct path to equilibrium crystals has been found by crystallization during polymerization [7]. This direct path involves polymerization of the monomers to the polymer crystals, bypassing the random coil macroconformation. A larger number of such reactions ranging from organic to biological to inorganic chemistry are known, including the polymerization of selenium, cellulose, and metaphosphates [1, Sect. 6.4].

2.3. Conformational motion in PE

The analysis of the measured and extrapolated C_p of crystalline and amorphous PE yields the three integral thermodynamic functions *H*, *G*, and *TS*, as illustrated in Fig. 6 [2–4,27]. On cooling through the glass transition, the mobile phases freeze to metastable, solid states and the functions *G* and *S* retain little meaning since they apply to equilibrium only.

When comparing C_p fitted to the vibrational spectrum of Fig. 1 to the measured and extrapolated C_ps, it was noted that the latter deviates gradually to higher values with temperature, starting already at 120 K for the PE glass, displayed in the left graph of Fig. 7A [44]. Making use of the observation of NMR line-broadening and the known energetics of the trans-gauche conformations on changing from torsional vibrations to large-amplitude, conformational motion, this deviation could be quantitatively matched to the shaded area in Fig. 7A. The rapid, isolated conformational motion

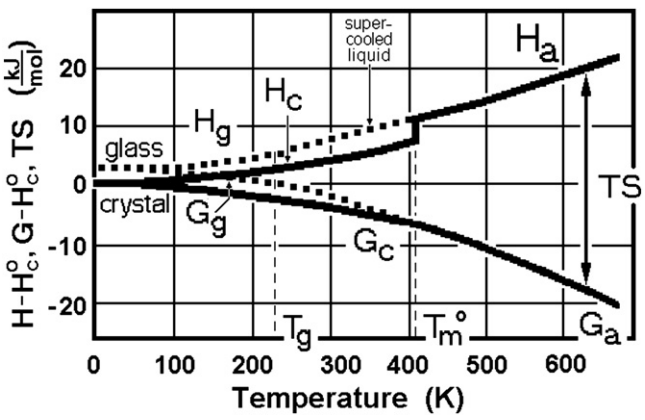

Fig. 6. Integral thermodynamic functions *H*, *S*, and *G* of crystalline (c), liquid-amorphous (a), and glassy (g) polyethylene [1]. Also shown are the glass and melting transition temperatures, T_g (237 K) and T_m° (414.6 K).

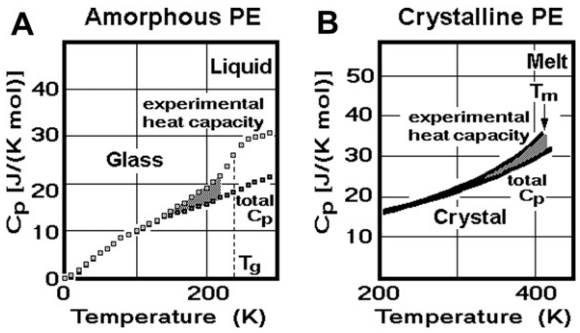

Fig. 7. Comparison of the contribution to C_p of the large-amplitude motion in glassy polyethylene (A) and crystalline polyethylene (B), marked by the shaded areas. The 'total C_p' refers to the vibrational heat capacity with $\Theta_3 = 80$ K for the glassy PE and $\Theta_3 = 158$ K for the crystalline PE (see Fig. 1).

changes above 200 K to the cooperative motion of the glass transition, centered at 237 K and completed at ≈250 K. At the time of this investigation, many qualitative estimates of the glass transition had appeared in the literature, placing the glass transition of PE erroneously in the temperature region from 140 to 200 K, i.e., in the region of isolated, large-amplitude motion. The error of such interpretations was addressed in [45], but has still not been fully removed from present-day's literature. The change from isolated gauche-trans defects to the cooperative motion defines the glass transition. It is caused by the decrease of activation energy for the simultaneous motion of neighboring conformations when compared to their separate motions, as detailed for the example of paraffins in [39, Sect. 2.2].

The same isolated, large-amplitude motion is observed in other mesophases of small and large molecules. Such mesophases frequently have heat capacities close to or even above that of the liquid state, signifying a continuous change of order starting below the transition temperature [39]. Even crystalline PE has an increasing number of mobile gauche conformations above room temperature (equilibrium defects), as shown in Fig. 7B. The same observation of a gradual C_p-increase beyond the vibrational C_p was also made on paraffin crystals [46] and could be linked to detection of the gauche conformations by IR analysis [47] and also to dynamic mechanical simulation of the crystals [40]. In PE and paraffins this motion does not reach the cooperativity of a glass transition below T_m, but for the higher-melting aliphatic nylons, a glass transition in the paraffinic regions of the crystals is possible [48]. Furthermore, glass transitions in equilibrium crystals were seen in poly(oxyethylene) crystals [49]. Such separate T_g below T_m is marked in Fig. 2 as a possible transition within the box of the crystal phase. It now links the four *solid* glasses at the top of the diagram to their four condensed *mobile* phases at the bottom with *crystals* in the center, eliminating structural order as the sole element determining solidity [50].

2.4. The oriented noncrystalline phase of PE

The coupling of the crystals to the surrounding amorphous phases in semi-crystalline polymers broadens the glass transition of the amorphous phase to higher temperature. For PE, however, one cannot observe a completed, separate RAF glass transition [51]. A surface layer of limited mobility between the crystal lamellae and the amorphous PE was identified with element-specific transmission electron microscopy. This layer is attached to the crystals and accepts a lesser amount of a RuO_4 stain. It was estimated to amount to 20–30% of the total mass [52]. Similarly, with solid state ^{13}C NMR, ≈20% of an amorphous interphase of 3.6 nm domain size

with limited backbone mobility was identified in HDPE [53]. Later, a semi-rigid interphase was found to surround the orthorhombic crystals in mPE copolymerized with 12.5 mol-% of 1-octene in which the copolymer units are fully rejected from the crystals [54]. Finally, in gel-spun fibers of UHMMPE, the interphase of limited mobility was shown to retain some orientation from the mechanical deformation. These highly-drawn fibers consist mainly of orthorhombic crystals and the oriented, noncrystalline phase (mesophase?) which is kept metastable by being coupled to the crystals. In addition, there are small amounts of monoclinic, hexagonal, and MAF. The latter three phases have little influence on the mechanical properties because of their low concentrations, but they do influence reorganization and melting [55]. The analyses consisted of calorimetry, full-pattern and small angle X-ray scattering [56], and the molecular motion was derived from solid state NMR [57].

Fig. 8 illustrates the difference of C_p for highly-drawn UHMMPE from that of the vibrational C_p (see Fig. 1) and equilibrium crystals. The glass transition range separates three regions of mobility. The first, below 190 K, agrees largely with the vibrational C_p (see the data points with the enlarged ordinate in the upper part of Fig. 8). Between 190 and 290 K there is a continuous increase in C_p of the fibers (ΔC_p) over that of the extended-chain crystals, indicating the broadened glass transition region of the noncrystalline content. Finally, there is the beginning of gradual crystal disordering, developing into a melting peak at about 375 K. The chemical shift of the NMR is the same for the carbon atoms of the orthorhombic crystals and the intermediate phases. The mobility of the intermediate phase, however, is 15 times higher than in the orthorhombic phase, as can be seen from Fig. 9 [57]. Their conformation is that of zigzag chains with imperfect lateral packing. The intermediate phase contributes significantly to the meridional X-ray diffraction peaks, but not to the equatorial ones. In the fiber direction the domains which consist mainly of the intermediate phase are much longer than the orthorhombic ones, which are more often interrupted. The overall tensile strength is thus mainly determined by the mass fraction and orientation of the intermediate phase [56].

The increases in heat capacity of the fibers in Fig. 8 corresponds to a noncrystalline content of 48% and does not agree with the calorimetric or volumetric crystallinities (77 and 88%, respectively) and certainly does not agree with the intensity of the crystalline X-ray scattering. To match all fractions (amorphous, oriented noncrystalline, and crystalline), one must assume that the oriented,

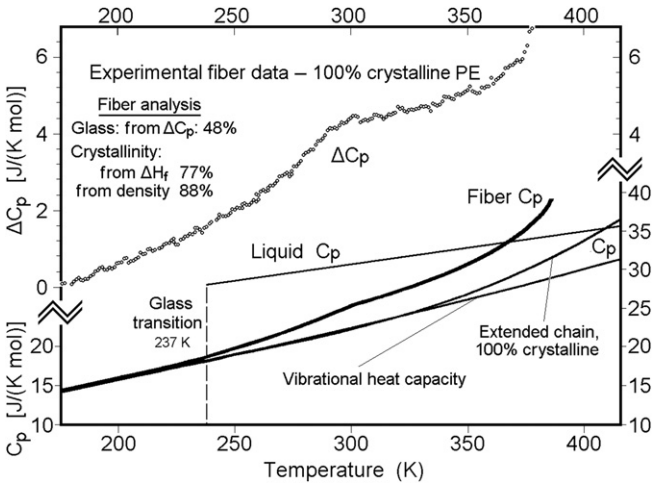

Fig. 8. The heat capacity of gel-spun UHMMPE fibers (reproduced with data from [55]).

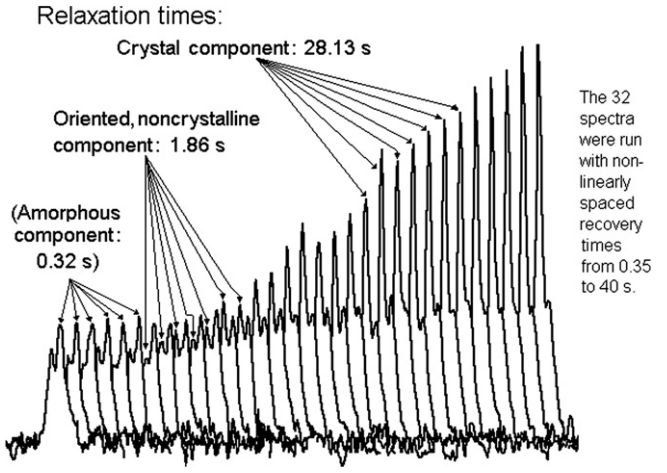

Fig. 9. A series of ^{13}C NMR spectra of a gel-spun PE fibers at different recovery times [57]. (Measurements of the spin-lattice relaxation times at room temperature using magic-angle spinning and high-power proton decoupling applying the progressive saturation method.).

noncrystalline phase has a heat of isotropization of ≈34% of the heat of fusion of the orthorhombic crystals, ΔH_f. This heat of isotropization changes with different thermal and mechanical histories of the fibers, proving that the oriented noncrystalline phase is not the same as the high pressure condis phase of PE.

2.5. The amorphous phases of PE

Above T_m, in the temperature range of the equilibrium melt, the amorphous phase of PE is easily studied. Compared to other flexible macromolecules, PE crystallizes quickly, so that the range of supercooling for HDPE liquid reaches down to only ≈400 K [58]. Data, down to T_g, must then be extrapolated as function of temperature or crystallinity [4] to obtain Fig. 6.

To keep PE liquid to lower temperatures, it was first attempted to eliminate heterogeneous primary crystal nucleation. By dividing the melt into microdroplets suspended in an inert medium, crystallization on cooling can be avoided down to about 360 K in all but the few droplets which contain a heterogeneous nucleus. Beyond this temperature, about 60 K below the equilibrium T_m, crystallization is speeded up by homogeneous nucleation [59].

Fig. 10 illustrates that with increasingly faster cooling experiments the crystallization is shifted to lower temperature. The first set of data were obtained with standard differential scanning calorimetry (DSC) and could be used for measurement of C_p of the melt down to about 390 K. The fast DSC of the second set could extend these measurements to 380 K. Finally, the recently developed fast scanning calorimetry (FSC) [60–64], based on chip technology, could push this value to 355 K by cooling at a rate of 5×10^3 K s^{-1}. Attempts at cooling UHMMPE at 10^6 K s^{-1} pushed this limit to ≈320 K [61,62]. A much reduced amount of crystallization could be seen before reaching the end of the glass transition [60] which is seen in Fig. 7A at ≈250 K.

A special quenching technique was developed earlier by shooting a molten, 10–100 nm thick polymer films into a mixture of solid and liquid nitrogen at ≈63 K. Electron microscopy and diffraction of the films without warming suggested an amorphous phase with 10 nm nodular superstructure [65,66]. Qualitative DSC on PE gave evidence for a cold crystallization exotherm at 160–200 K [65]. These experiments make it likely that glassy PE starts to crystallize in the temperature region of local large-

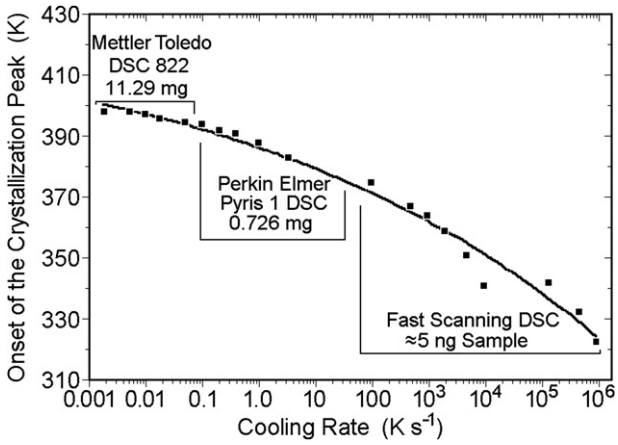

Fig. 10. Non-isothermal crystallization of UHMMPE. Peak onset temperature in a wide range of cooling rates achieved by combining data from three calorimeters. Data from [60,61]. The line is a guide for the eyes.

amplitude motion (see Fig. 7A). On fast quenching, this means the temperature of first cold crystallization must be traversed faster than accomplished in Fig. 10.

To summarize the phases of PE, there is an orthorhombic phase, stable below the equilibrium T_m of 414.6 K and a less stable monoclinic phase, frequently found as a fraction of the crystals grown on drawing of fibers or films, rolling, and melt extrusion. At elevated pressure, a hexagonal condis mesophase becomes stable (see Figs. 4 and 5), unrelated to the paraffin mesophases at atmospheric pressure which become unstable at higher pressure. The bulk-amorphous phase has a broad glass transition, starting at about 120 K with local, large-amplitude motion which becomes cooperative at higher temperature with a T_g at 237 K. There is a restriction of the large-amplitude motion in the amorphous layer around the crystal due to coupling through tie molecules, broadening the glass transition to higher temperature. On deformation, this layer becomes an oriented, noncrystalline phase which governs the fiber properties, but is metastable only under the constraint by the crystals. Although not studied in as much detail, such oriented, noncrystalline phases, created by external mechanical deformation are expected to be present in most other semi-crystalline, flexible, linear macromolecules.

3. The phases of isotactic polypropylene (iPP)

3.1. Polymorphism and morphologies of isotactic polypropylene

Isotactic polypropylene (iPP) exhibits different crystal structures and morphologies as a function of crystallization conditions [67,68]. Cooling the melt at low or moderate rates results in monoclinic α-crystals ($P2_1/c$, sometimes also called form I), with details given already in 1960 by Natta and Corradini [69]. The molecules adopt the lowest energy helix (2*3/1) which is not part of the crystal symmetry, as in iPB. The symmetry elements are shown in Fig. 11 and can be compared to iPB form I. The 2*3/1 helices, as displayed in Fig. 3 for iPB, are aligned parallel to the crystallographic *c*-axis which comes vertically out of the plane of the paper and, as common for helices, left-handed and right-handed helices achieve closest packing as nearest neighbors [1, Fig. II.33]. Because of the relative smallness of the methyl side group, even closer packing can be reached in iPP than in iPB by contacting two isochiral helices in addition to three nearest neighbor helices of opposite chirality. This leads to the crystallographically rare coordination number five for the helices of the monoclinic iPP crystals.

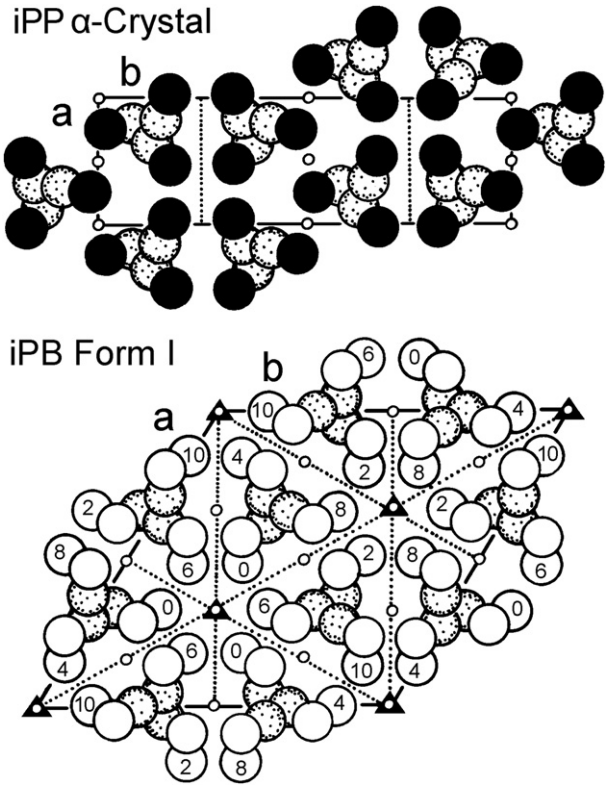

Fig. 11. The unit cells of the stable crystals of iPP (α-crystals, monoclinic) and iPB (form I, trigonal). For iPP: The 2*3/1 helix axes of the molecules are not part of the crystal symmetry. The two sets of twofold screw axes, 2_1, (¼) parallel to *b* have been left out for clarity. In space group $P2_1/c$, helices related by the left glide plane should be isoclined, 'up', and those by the right glide plane, due to the centers of symmetry, 'down', or vice versa. Drawn after [1, Fig. II.41]. For iPB: The glide planes *n*, located between the marked *c*-glide planes and the twofold rotation and screw axes in the *ab* planes have been left out for clarity. Elevations of the CH_3-group are in units of *c*/12. The threefold screw axes 3_1 and 3_2 of the crystal coincide with the 2*3/1 helix axes of proper sense of rotation (also not indicated). Glide planes are marked by ⋮, centers of symmetry by °, and three-fold rotation axes by ▲.

Major crystal defects are caused by helix segments of wrong handedness. Lesser loss of thermodynamic stability arises from a disorder in the inclination of the methyl groups of neighboring chains (up/down defects) in violation of the crystal symmetry [70]. Ultimately, a continuum of modifications of the α-polymorph was described for samples annealed >420 K. Depending on thermal history and crystallization conditions this may increase the observed melting by up to 15 K [71]. A 'limit-ordered' α_2 monoclinic crystal form with only 5–10% of defects is obtained at the highest crystallization or annealing temperatures [72].

The superstucture of the melt-grown monoclinic crystals is spherulitic, with the lamellae displaying a unique branching [73–75]. Epitaxial growth of daughter lamellae on the base lamella leads to the so-called cross-hatching, i.e., the spherulites contain both radially and tangentially oriented lamellae.

Two other major polymorphs of iPP (β and γ, or forms II and III) were first studied by Turner-Jones [68]. An in-depth analysis of the spherulitic structure and the birefringence pattern of different semi-crystalline iPPs by Keith and Padden in 1959 enabled classification of the β-polymorph as a pseudo-hexagonal crystal structure [76,77], further investigated in the mid 1990s by Meille [78] and Lotz [79]. Crystallization from the quiescent supercooled melt in presence of special nucleators favors the β-form [80] and is technically important for preparation of iPP with specific mechanical properties arising from the absence of cross-hatching of lamellae [81,82].

The γ-structure develops preferentially in the presence of chain defects which limit the isotactic sequences, in low molar mass fractions, or during crystallization at elevated pressure [83,84]. The unit cell is orthorhombic with adjacent bilayers of chain segments with a relative tilt of 81°. Furthermore, chains are oriented at an angle of 40° normal to the basal plane of the lamella [85,86]. Research about the conditions of the formation of γ-crystals has recently intensified by analysis of the structure of random propylene-1-alkene copolymers [87,88].

The mesophase of iPP can be considered a fourth polymorph and will be discussed next. Regarding the various crystal structures just introduced, only the monoclinic α-structure which is closely related to the mesophase will be considered further.

3.2. Condition of mesophase formation

Crystallization of iPP by quenching from the melt leads to a mesophase [89,90]. By 1984, the mesophase was identified as being metastable and conformationally disordered, listed in Fig. 2 as a CD glass [91] (condis crystal below its T_g). Earlier suggestions of 'paracrystalline' or 'smectic' crystals could not be substantiated (but the erroneous nomenclatures, labeling the iPP mesophase as 'paracrystalline' or 'smectic' have unfortunately not been fully removed from the present-day literature). Many calorimetric measurements have led to the equilibrium functions for liquid (melt and supercooled melt) and solid (crystalline and glassy) iPP [3,91,92].

In this early period of thermal analysis, the mesophase was studied in several ways:

1. The quiescent melt was cooled at rates of up to 70 K s^{-1} to investigate the conditions of growth of the mesophase [93].
2. Annealings of the mesophase were done at increasing temperatures to test its stability [91].
3. Partially grown monoclinic crystals were quenched to continue ordering of the only partially crystallized samples at low temperature [93].
4. Cold crystallization of the mesophase was attempted after partial devitrification of the glassy, amorphous fraction of semi-crystalline, monoclinic iPP samples [91].

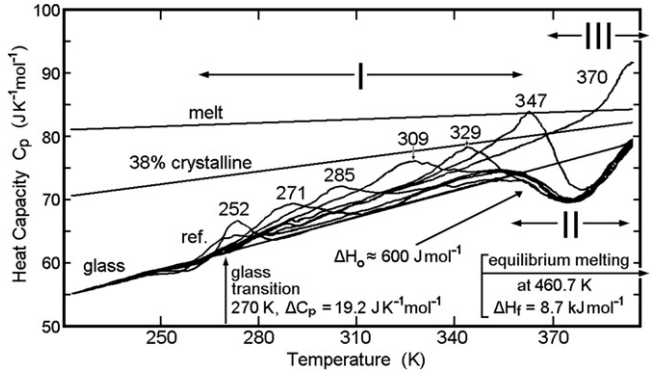

Fig. 12. The heat capacity of partially condis-crystalline iPP at a heating rate of 50 K min^{-1} (= 0.83 K s^{-1}). The measurements were made after quenching the sample in the calorimeter with liquid nitrogen which resulted in the mesophase with a heat of fusion corresponding to a crystallinity of ≈38% (curve labeled 'ref.'). The additional samples were annealed for 180 s at the indicated temperatures (in K). Also shown are C_p of the glass (solid), the extrapolated melt, and a 38% crystalline sample [3]. Redrawn from [91, Fig. 4]. Note, that the temperature-ranges I and II overlap, they involve mesophase melting and transition to the monoclinic phase. Range III, refers to perfection and melting of monoclinic crystals. It extends into range II and continues to the completion of melting (not shown).

Experiments (1) showed that the growth of the mesophase below ≈350 K is rapid down to 280 K, close to the T_g of bulk iPP, 270 K (value of the ATHAS Data Bank [3]).

Experiments (2) revealed from the overall latent heats that the reference mesophase before annealing had a crystallinity of ≈38%. In Fig. 12, it can be seen that the semi-mesomorphic sample (labeled 'ref.') shows up to the exotherm in temperature range II little or no increase of C_p beyond the vibration-only level of solid iPP, i.e., the mesophase coexists in this temperature range with an RAF, but seemingly, there is little or no MAF. This led to the conclusion that the mesophase itself had to be a CD glass (see Fig. 2). After annealing at the indicated temperatures in Fig. 12, small endothermic maxima developed somewhat above the annealing temperatures in the temperature region I which covers approximately 100 K. These were suggested to be melting peaks of some additionally grown mesophases of very small sizes, so-called 'annealing peaks'. Their peak sizes increased with annealing temperature and moved to higher-melting temperatures. This additional mesophase grown at the annealing temperature did not exceed 2–3% crystallinity. On annealing up to ≈340 K, all additionally grown mesophase had melted before reaching the transition exotherm in region II of the condis glass. The additional mesophase, grown on annealing in region I, remains devitrified (MAF) after its low temperature melting. In region II, helix mobility starts, as known from NMR data (beginning at 360 K [94]). The mesophase becomes unstable and converts to the monoclinic crystals with a latent heat of ≈7% of the monoclinic heat of fusion. Ultimate fusion of all monoclinic crystals occurs in region III, and its peak is commonly reported at ≈420–430 K.

The experiments (3), carried out between 398 and 408 K, involved the interruption of the growth of monoclinic crystals, followed by mesophase crystallization after quenching to lower temperature. These measurements are displayed in Fig. 13. They were designed to possibly detect a temporary layer of mesophase during the growth of monoclinic crystals, thought to occur on ordering of short 2*3/1 helix segments which are known to be present already in the melt [95]. Fig. 13 shows no indication of such intermediate mesophase during crystallization at 403 K. If there had been an intermediate mesophase growing as precursors to the monoclinic crystals, it should have produced data points above the straight line diagonal. On the contrary, the data lie below the straight line and indicate that monoclinic growth at 403 K hinders subsequent mesophase formation, most likely by the RAF coupled to the monoclinic crystals.

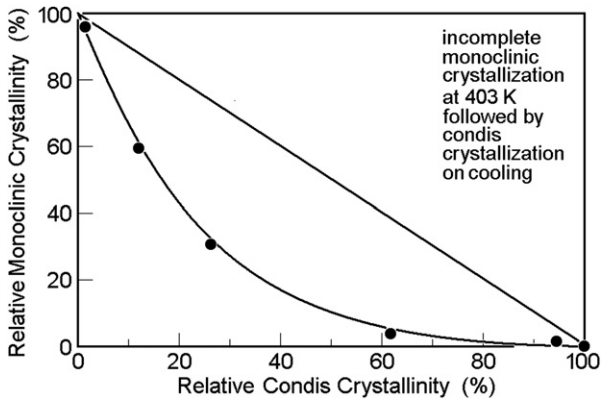

Fig. 13. Example of relative crystallinities obtained in two-stage crystallizations (redrawn from [93, Fig. 5]). The monoclinic crystallinity was measured up to the time of interruption at 403 K and recalculated as percentage of the finally observed heat of fusion (after conversion of the later grown condis phase to monoclinic crystals during the DSC analysis). The condis crystallinity was measured during the subsequent fast cooling from 403 K at ≈70 K s^{-1} and is expressed as percentage measured when cooling without stopping for growth of monoclinic crystals at 403 K (point at 100%).

Experiment (4) is illustrated with Fig. 14. A sample of ≈52% monoclinic crystallinity was reheated and annealed for 3 min at 370 K, inside the temperature region II of the exotherm on Fig. 12 where the mesophase is unstable. The annealing was followed by quenching. On subsequent analysis, one can see a normal glass transition of bulk-amorphous iPP, followed by about 6% cold crystallization (ΔH_2) of an intercrystalline mesophase which melts right thereafter at 340 K, so that there is no exotherm that should be present when any mesophase changes to monoclinic crystals. The melting temperature for the cold-crystallized mesophase grown between 280 and 320 K with the heat of fusion ΔH_3, thus, is ≈330 K. This agrees with the annealing peak in the temperature region I of Fig. 12 labeled 309 K which occurred at ≈320 K. The melting of the monoclinic crystals in region III was unchanged by the annealing in region II.

Recently 30–40 nm small phases of iPP could be analyzed by standard DSC on cooling from the melt. They were produced by the brake up of ultra-thin iPP films stacked between polystyrene films [96] and by dispersion of graft copolymers of iPP with maleic anhydride in water [97]. For sizes approaching nanophase dimensions [98,99], heterogeneous nucleation was insignificant, and mesophase formation on cooling from the melt occurred at rates as slow as 5–10 K min^{-1}! The subsequent DSC heating traces of the mesophases were comparable to the earlier studies [91,93], but not referred to in [96,97], so that a proper interpretation of the mesophase was not made and more quantitative comparisons were not attempted.

Also, in the meantime, the cooling and heating rates could be increased substantially. Piccarolo and coworkers studied cooling and supercooling of iPP and investigated the phase structures by X-ray diffraction and dilatometry. Films of 100 μm thickness were solidified with non-linear cooling rates from 10^{-1} to 10^3 K s^{-1} [100–103]. Fig. 15 shows a typical density plot for varying cooling rates. The cooling rates were achieved by applying cold water in ballistic quenching experiments on the thin films. Cooling at rates less than 50–100 K s^{-1} resulted in formation of semi-crystalline structures with densities of 0.900–0.910 g cm^{-3} (region A). Cooling rates higher than 10^2 K s^{-1} led to densities between 0.885 and 0.890 g cm^{-3} (region B), X-ray data revealed that the latter samples contained only mesophase and amorphous iPP.

Further progress was made by combining standard DSC and FSC to cover a wider range of cooling rated [104–107]. The FSC allowed analysis on cooling between 15 and 10^3 K s^{-1} by linear cooling down to sub-ambient temperatures. The data are presented in Fig. 16. Between 390 and 348 K semi-crystalline iPP of monoclinic structure was observed (region A). With cooling rates of 80–300 K s^{-1}, the formation of partially ordered mesophase was observed at distinctly lower temperatures, between 313 and 293 K (region B).

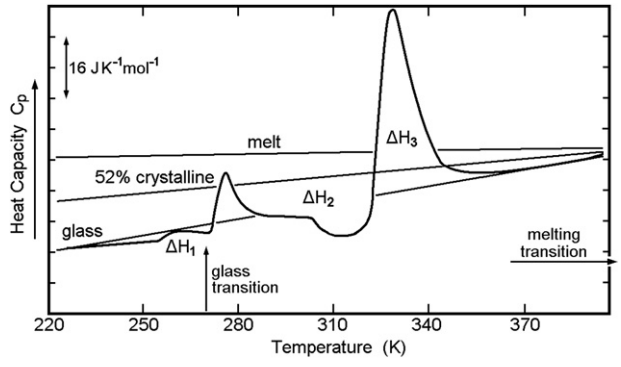

Fig. 14. DSC curve measured by heating at 50 K min^{-1} of a semi-crystalline iPP grown by cooling at 0.5 K min^{-1} from the melt, followed by annealing for 3 min at 370 K before quenching for the measurement. The areas ΔH_2 and ΔH_3 correspond to cold crystallization and melting of ≈6% condis crystallinity [91].

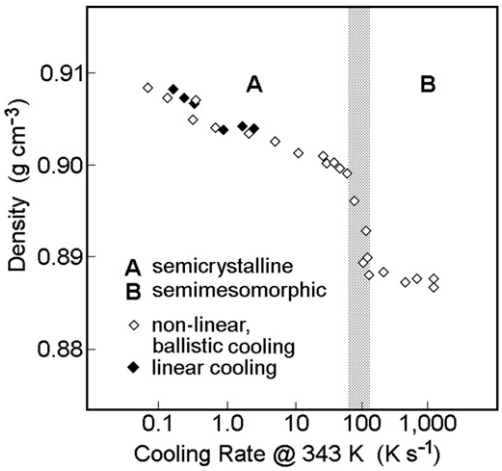

Fig. 15. Density of iPP as a function of cooling rate on solidification of the quiescent melt. Adapted with permission from [103]. Copyright 2002, Elsevier.

It is interesting to note that homogeneous nucleation of iPP starts below ≈355 K, ≈105 K below T_m° [96,108]. Further increase of the cooling rate to 10^3 K s^{-1} suppresses the mesophase formation on cooling below the bulk-amorphous T_g. Ageing of such amorphous iPP at ambient temperature always results in mesophase growth, regardless of the prior cooling rate.

The FSC has also been employed to evaluate overall rates of isothermal crystallization as function of temperature between 273 and 373 K [106] and 258 and 363 K [107]. Fig. 17 is a plot of crystallization time, measured by the time to the peak of the exotherm on isothermal crystallization (the approximate half-time of crystallization) [106]. There are two minima, one at 293–303 K and one at 353–363 K, corresponding to maximum rates of growth of the mesophase and the monoclinic crystals, as confirmed earlier by non-isothermal FSC [104,105].

The time for monoclinic crystallization in Fig. 17 seems to follow the standard interpretation [1, Chapters V and VI]: At high temperature, the crystallization time increases and ultimately goes to infinity, caused by the need of nucleation, governed by the activation energy to create a critical nucleus. At low temperature, the molecular, large-amplitude motion in the melt slows, and

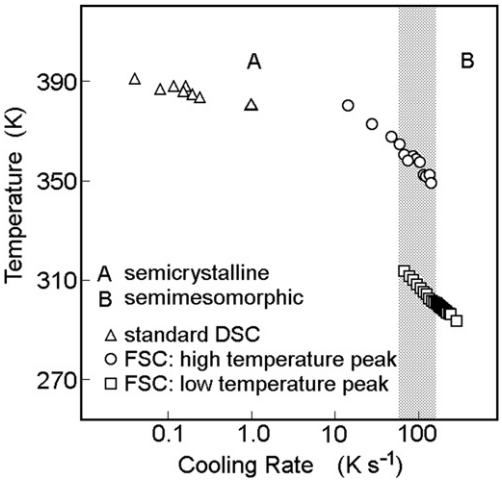

Fig. 16. Crystallization peak temperature of iPP as a function of cooling rate. Adapted with permission from [105]. Copyright 2006, American Chemical Society.

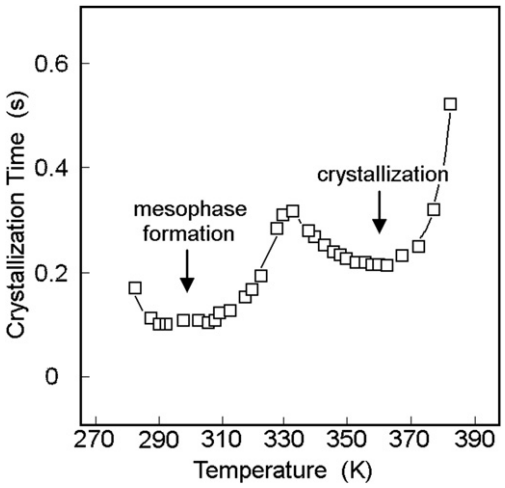

Fig. 17. Crystallization time as a function of temperature of isothermal crystallization of iPP [106]. Copyright Wiley-VCH Verlag & Co. KGaA. Adapted with friendly permission. The time was measured at the peak of the exotherm and is approximately the half-time of crystallization.

ultimately terminates crystallization when the glass transition is approached.

The question arising out of Fig. 17 is then: Why is the upturn in crystallization time at low temperature starting at 350 K, 80 K above T_g of bulk-amorphous iPP, when for the mesophase formation, it starts only at 290 K? There may be more than one answer.

One answer may be that the mesophase formation is hindered by T_g of the bulk-amorphous iPP, but the monoclinic crystallization is slowed already by the beginning of the glass transition of its RAF at $\approx$320 K (at 0.8 K s^{-1} [91]). An extreme example of such hindering of crystallization was discovered for poly(oxy-2,6-dimethyl-1,4-phenylene), PPO. Crystals of PPO (and its nuclei) produce an RAF with a T_g above T_m, hindering crystallization from the melt. Substantial crystallization in PPO, accordingly, occurs only in the presence of diluents which softens the RAF. After removal of the diluent, the crystals remain metastable beyond their T_m and melt only in concert with the gaining of large-amplitude motion of the RAF at T_g [51]. Other examples of bimodal crystallization rates studied by FSC were found for poly(butylene terephthalate), PBT [109], and poly(ε-caprolactone), PCL [64].

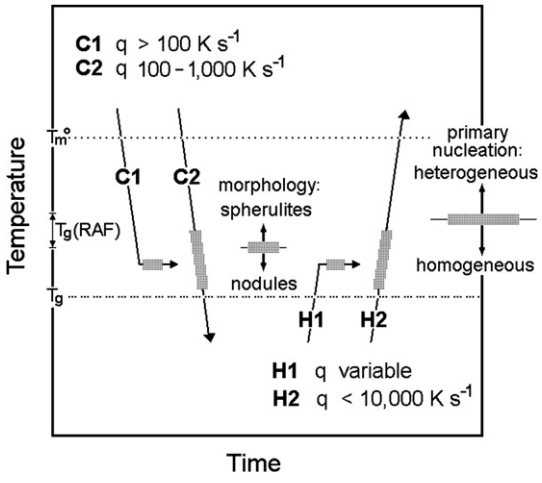

Fig. 18. Schematic of the time-temperature conditions of mesophase formation of iPP (shaded sections along curves C and H). The limits of the rates of temperature change, q, are indicated in the figure, but according to [96,97] change when the size of the phases decrease below $\approx$50 nm. Marked on the temperature scale are T_m° and T_g of the bulk-amorphous iPP and the temperature range of T_g (RAF). The limits of morphology and primary nucleation are also indicated.

Another reason for the bimodal overall crystallization time may be the change from limited heterogeneous, to overall homogeneous nucleation which occurs in this temperature region [96,108]. On homogeneous nucleation, nuclei form anywhere and may overcome the decreasing linear growth rate due to the increasing global viscosity. Separate information on primary nucleation rate and linear crystal growth rate could prove such reasoning. The frequent nucleation is also a link to the nodular morphology which enhances intramolecular ordering in the size range of the random coils, as discussed below in Sect. 3.4 with Figs. 19 and 20. These examples indicate that the 'classical' nucleation model of Turnbull and Fisher [110] governed by supercooling and glass transition of the MAF alone [1, Sect. 5.1.2] needs to be modified in the presence of RAF [111]. Ultimately the rate of molecular nucleation [1, Sect. 5.3] and the rate of reversible crystallization on the growth face must also be considered [51]. All of these mechanisms are ultimately influenced by the coupling of amorphous and ordered portions within the molecules which bridge the different phases [8] (see also Sect. 2.4).

A summary of the condition of mesophase formation of iPP is shown in the schematic of Fig. 18. The mesophase crystallinity can reach levels similar to the monoclinic semi-crystalline samples. From a supercooled bulk iPP melt, mesophase grows below the change from heterogeneous to homogeneous nucleation and the glass transition range (covering RAF of mesophase and crystals and also the CD glass). Thus, the mesophase may develop by quick cooling from the melt (paths C), or on heating from the amorphous glass (paths H). Avoiding crystallization of monoclinic iPP, path C1 requires cooling faster than 100 K s^{-1}. Non-isothermal mesophase formation requires either a cooling from the melt at a rate between 10^2 and 10^3 K s^{-1} (path C2), or heating from the amorphous glass at a rate of no more than $\approx 10^4$ K s^{-1} (path H2). All ordering is avoided for C2 with rates above 10^3 K s^{-1} or for H2 with rates above 10^4 K s^{-1}. Changes in rates for very small phases (<50 nm) were mentioned above.

3.3. Structure of the mesophase

The mesophase of iPP contains parallel helices of different handedness [89,90], with the same 2*3/1 helix as seen in the crystalline polymorphs, confirmed by infrared spectroscopy [90,113] and wide-angle X-ray scattering (WAXS). The mesophase is recognized in the WAXS pattern by presence of two characteristic halos. One at a spacing of about 0.59 nm, related to the distance between parallel aligned chains in the mesophase, and the other, at a distance of 0.41 nm, assigned to the repeating period within the helices [114,115] (see also Fig. 21, below). To account for a hexagonal crystal symmetry, different interpretations of the WAXS data of quenched iPP were suggested. One interpretation assumed the presence of small crystallites of hexagonal structure [66,116–118], but in the mesophase the lateral local correlation of chain segments was found to be closer to monoclinic than hexagonal [119–121]. It was, however, confirmed that the mesophase contains bundles of 2*3/1 helices, aligned parallel, but being terminated in direction of the chain axis by helix reversals or other conformational defects.

All these structure suggestions did not consider the conformational motion (see Sect. 1.2). It would average the involved structure elements over time, or in a CD glass with frozen conformations, produce an average structure of short chain length segments not resolved by the X-ray analysis. In both cases, a higher (average) symmetry results. A similar averaging of the chain conformations exists also for PE and the paraffins (see Sect 2.2), as well as for iPB (see Sect 4.2). Despite being conformationally disordered, the

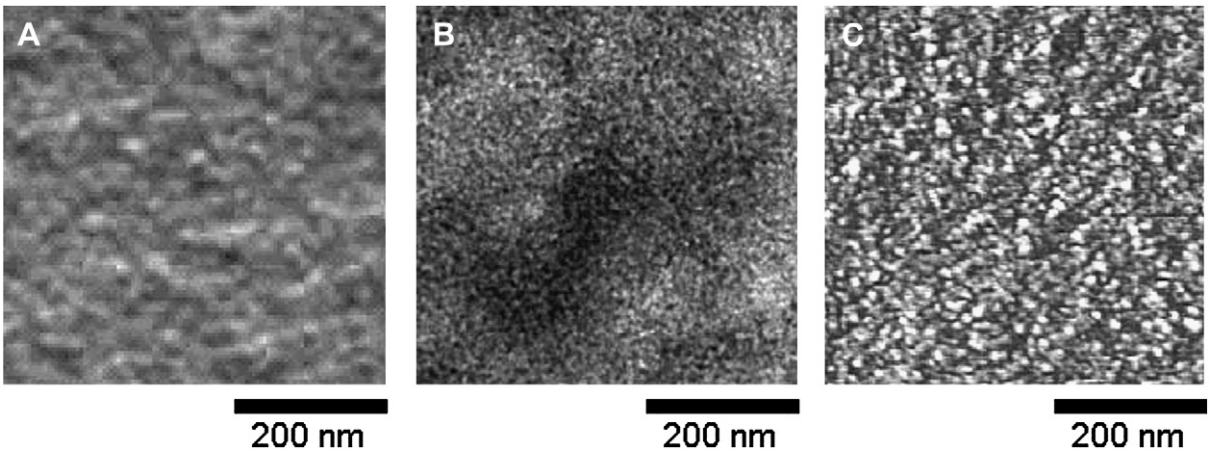

Fig. 19. Morphology of the mesophase of iPP as obtained by TEM (A and B) and AFM (C). The originally published images were modified and are reproduced with kind permission: (A) by John Wiley & Sons, copyright 1968 [66]; (B) by Elsevier, copyright 2001 [128]; and (C) by Springer Science + Business Media, copyright 2008 [131, Fig. 2(left)].

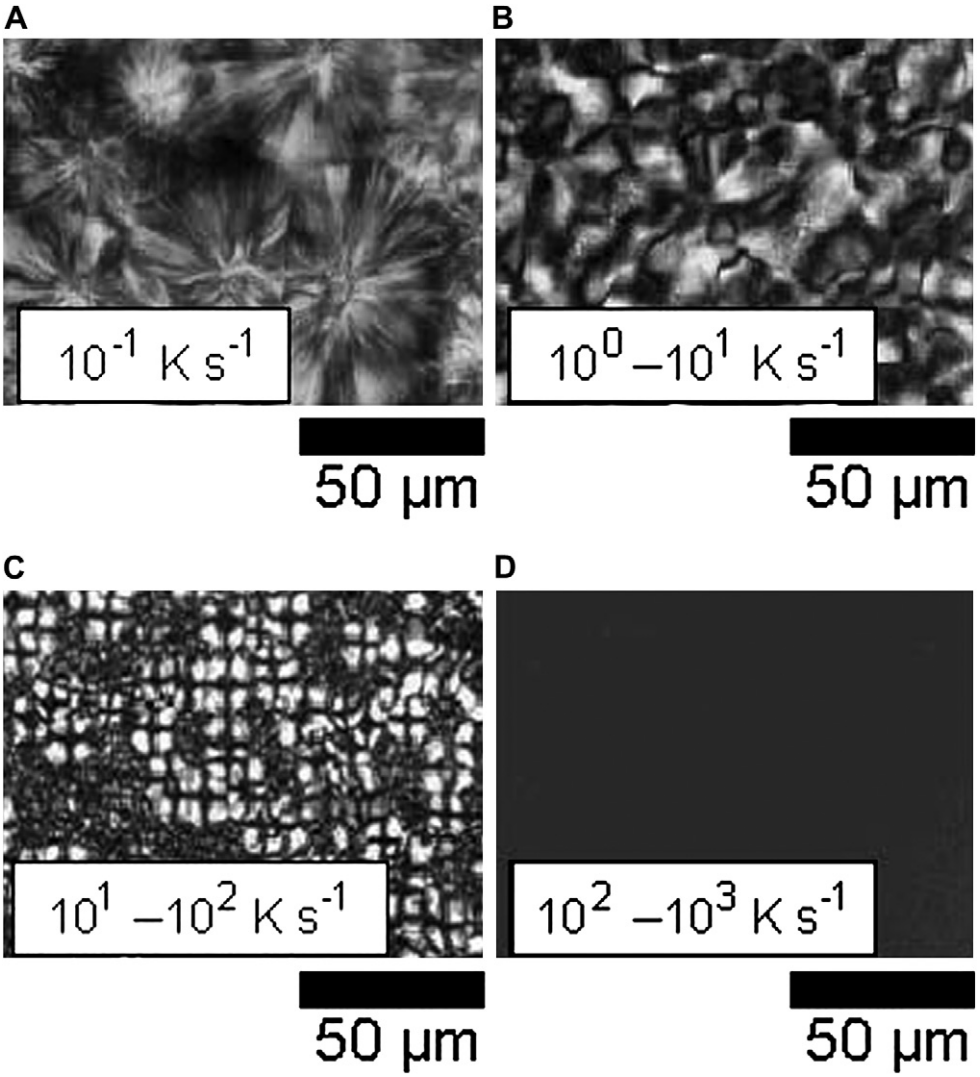

Fig. 20. Optical micrographs with polarizing light of films of iPP of 100 µm thickness, showing a spherulitic superstructure after cooling at a rate lower than 100 K s^{-1} to ambient temperature, and the absence of such superstructure on quenching at a rate faster than 100 K s^{-1}. Adapted from [130], copyright 2006, and [138], copyright 2009, with permission from Elsevier.

mesophases would exhibit long-range positional and orientational order between the helix segments.

3.4. Morphology and habit of the mesophase of iPP

Fundamental, early work regarding the morphology of the mesophase of iPP has been carried out by Geil and coworkers [66,112]. Ultra-quenched films were heated to room temperature where electron microscopy showed a surface structure composed of nodules of sizes between 7.5 and 10 nm. Similar nodular habits have been observed after quenching of amorphous PE (see Sect. 2.5) and were retained during initial, low temperature crystallization, but ultimately changed to spherulites, consisting of crystals of the common lamellar habit. The crystallization of the glass of amorphous iPB [122] and other polymers, such as poly(ethylene terephthalate) [123], also revealed similar morphologies. To put the nodule size into perspective, one can compare it to a random coil of the analyzed polymer in the melt. The typical iPP analyzed in the quoted researches had a molar mass of 250–500 kDa, i.e., the root mean square distance from the center of gravity is 16–23 nm (as estimated from an unperturbed chain with a Kuhn length of 0.37 nm instead of the bond length of 0.154 nm [2]).

These observations of nodular morphology in quenched samples crystallized from the glass were originally thought to be related to instrumental artifacts of the electron microscopy [124,125]. By now, however, the nodular morphology of ordered domains in quenched and subsequently annealed iPP at ambient temperature has been confirmed in many studies with a variety of preparation techniques and instrumentations for imaging [126–133].

Fig. 19A–C show results of such investigations. Fig. 19A was obtained by transmission electron microscopy (TEM) on a 10 nm thin sample of iPP prepared by quenching with ice-water, and shadowing with platinum and carbon. The specimen was described in this investigation as showing a 'ball-like' or 'grainy' structure, with the grains having a size of 12.5 nm [66]. Fig. 19B resembles this structure. It was prepared by melt extrusion of a 0.25 mm thick iPP film on a chill roll at 281 K. The image was collected by TEM on sections of thickness of 70–75 nm, cut at ambient temperature. Before cutting, cryo-faced specimens were stained using the vapor above a RuO_4 solution. The specimen was described as containing 'cluster-like' structures with an average size of 10 nm. The darker and brighter regions were described as amorphous (more heavily stained) and mesomorphic (less stained) [128]. Fig. 19C was produced by atomic force microscopy (AFM) on a specimen of 0.1 mm thickness which was cooled at a rate of 750 K s^{-1} to 279 K and subsequently aged at ambient temperature. The size of the domains are of the order of 15 nm, i.e., somewhat larger than those estimated from the TEM. The apparent mismatch seemingly results from interactions between sample and AFM tip. The AFM image collected with super-sharp tips yields smaller nodule sizes [132].

Further information about the domain size of quenched iPP, aged at ambient temperature, was gained by analysis of the line-broadening of WAXS after mathematical peak separation. They revealed a lateral crystal size of 3–5 nm [114,118]. In addition, small angle X-ray scattering (SAXS) was analyzed from their Bragg peaks. Typically, a long-period of about 10 nm was found in such investigations [128,133–137]. The nodules with a size of the order of 5–20 nm account for about 25–50% of the total structure of quenched and aged iPP [102,117,135] and are embedded in an amorphous matrix without superstructure of its own.

Fig. 20A–D contain optical micrographs taken between crossed polarizers of iPP cooled at the indicated cooling rates. The pictures of Fig. 20A–C, taken after slower cooling, show the typical spherulites of lamellar, monoclinic crystals. The fast cooled sample of Fig. 20D does not show any characteristic extinction pattern [100,130,138]. The nodular structure shown in Fig. 19, having the dimensions of a random coil, is of a scale invisible in Fig. 20, i.e., their size is smaller than the maximum resolution of the optical microscope. The typical diffraction limit of a microscope is 200 nm for green light (using oil immersion, NA ≈ 1.5). The decreasing size of the spherulites with increasing cooling rate between 10^{-1} and 10^{2} K s^{-1} is due to increasing nucleation density, in accord with the shape of the exothermic peak observed in isothermal calorimetry [107] and with the concepts of polymer crystallization [1, Chapters V and VI]. Fig. 20D illustrates that despite the considerable content of mesophase, there is no birefringent, multi-molecular superstructure when exceeding the cooling rate for the growth of monoclinic crystals given in Fig. 18 (path C-2). The absence of visible spherulites is indicative of the appearance of a large number of homogeneous nuclei or domains of ordering as one expects from the ordering of separate molecules in an isolated, homogeneously nucleated, fringed micellar crystal growth as reviewed in [1, Sect. 5.1.2.1]. The connection of the temperature range of mesophase formation with the transition temperatures, morphologies, and primary nucleation mechanism can also be seen from Fig. 18.

3.5. Stability and reorganization of the mesophase of iPP

The stability and reorganization of the mesophase of iPP can now be discussed using research on its calorimetry (see Figs. 12–14), dilatometry (see Fig. 15), temperature-resolved WAXS (see Fig. 21, below), solid state NMR [94], and microscopy (see Figs. 19 and 20). As long as the thermodynamic functions are available, calorimetry is the definitive method to assess the phase stabilities, as discussed in Sects. 2.1–3 for PE. In a plot such as Fig. 6 for PE, the stable state has the lowest Gibbs energy, G. The experimental C_p [3,91] was linked to the vibrational spectra for iPP, updated and compared to PE, iPB and a number of other branched macromolecules [27]. To establish G of equilibrium crystals of iPP, the connection must be made between the easily available equilibrium melt and the experimentally not yet realized equilibrium monoclinic crystals at the equilibrium melting temperature. The (extrapolated) equilibrium melting temperature and heat of fusion are $T_m = 460.7$ K and $\Delta H_f = 8.7$ kJ mol^{-1}, respectively [92]. Once the transition parameters are available, crystallinities can be calculated with help of the C_p of the solid state. Finally curves as given in Fig. 6 for PE, including the entropy contributions, could be completed [3,27].

The large-amplitude motion in iPP is characterized, as usual, by DSC in the glass transition region. For the amorphous phase, T_g was chosen to be 270 K, based on measurements of specially synthesized, completely random aPP samples without head to head sequences [139] and making the assumption that iPP has a closely similar T_g. The T_g for semi-crystalline iPP was observed at 272 K for the mobile amorphous fraction (MAF). This was separated from a less defined, broader second T_g of the RAF, reaching from ≈ 320 to 360 or even 380 K [91]. Measuring with FSC on cooling of iPP with a rate of 10^{4} K s^{-1}, sufficient to avoid crystallization, a T_g of ≈ 280 K was reported [60]. Considering the four orders of magnitude higher cooling rate than used in the earlier calorimetry, this seems to be somewhat lower than the T_g of aPP. The typically observed increases of T_g by DSC of amorphous polymers are 4–8 K per decade of heating rate [2, Sect. 6.3.1]. Lower values, down to 250 K are also frequently quoted, but usually measured on poorly characterized materials [92]. A detailed study of the T_g of iPP as a function of structural and stereo isomerism as well as molar mass and crystallization condition seems not available. The beginning of cooperative motion in aPP by solid state NMR was seen at 250 K. The beginning of helix mobility in monoclinic crystals of iPP, in

contrast, is 360 K [94]. The last value is the same as known for the 2*3/1 helices of iPB [140], i.e., both polymers are characterized by similar intramolecular motion involving gauche-trans interchanges.

Next, a linking of the calorimetry with molecular mobility, packing, structure, and morphology can be attempted. Below the glass transition, the C_p of all phases is practically the same and can be matched to an appropriate vibrational spectrum [27]. As seen in Fig. 1 for PE, the group vibrations and the upper skeletal vibrations (characterized by the Θ_1-temperature) account for most of the thermal energy from the molecular motion and changes little for the different phase structures. Below 50 K, the heat capacity is sufficiently small so that differences in the skeletal frequency spectrum are insignificant (characterized by different Θ_3-temperatures [2–4]). With a crystallinity of ≈38% for the eight samples used for Fig. 12, the beginning of the glass transition is in the region of T_g of the bulk-amorphous phase. All C_ps stay far below the level expected for 38% crystallinity (intermediate straight line), i.e., all samples have a broadened glass transition and most of the iPP remains rigid. The reference sample ('ref.' in Fig. 12) before and after annealing at 252 and 271 K suggests that the mesophase is a CD glass (see Fig. 2) and the RAF includes almost all amorphous iPP.

From the exotherm centered at 376 K, the heat of ordering of the condis crystals is ≈600 J mol^{-1} [2,3] (for 100% mesophase [91], discussed also in [1, Section 9.3.2.2]). This is much less than for ordering of the PE mesophase (≈65% of the ΔH_f of the crystals [39]). The recent data on small phase iPP [96] were within the error of the ATHAS Data Bank. New data on drawn iPP [141] led to only half of the ≈600 J mol^{-1}, perhaps indicating a better packing in the drawn mesophase, an observation that would go parallel with the gel-spun UHMMPE, which also developed 'crystallinity' in its oriented, noncrystalline phase (see Sect. 2.4, Fig. 8).

The exotherms in Fig. 12 signify a higher entropy and Fig. 15, a lower density within the mesophase. At low temperature, monoclinic iPP with lower entropy and better packing must then be the more stable phase. But, why then is the mesophases not the thermodynamically more stable high temperature polymorph and forms only at low temperature? The formation of a mesophase rather than the stable crystal can find its explanation in the 19th century 'law of successive states', formulated by Ostwald. It suggests that a new phase appears to go through stepwise changes from less to more stable polymorphs [1, Sect. 7.1.5]. This is a process, more recently suggested to also minimize the entropy production path of crystallization [142]. For macromolecules, however, ordering of the long molecules has to start obviously in short segments of the molecules. Depending on temperature, these ordered segments may produce RAFs coupled to the ordered regions. The RAF, in turn, may impede not only transport of new crystallizable segments to the growth face, but also hinder crystal perfection involving the extension of chain folds (see Sect. 1.1), the removal of helix reversals, and—more difficult—the correction of wrong inclinations (requiring recrystallization, as discussed in Sect. 3.1). This ordering after primary nucleation and initial growth commonly is gradual and does not normally lead to a well-defined mesophase. Ultimately, the ordering stops, when the MAF reaches a level determined by the formation of crystals and RAF. The same is true for removal of the defects (see, for example [143], and also the discussion of fold lengths and block formation [144]).

For iPP, the similarity of the T_g of the RAF and the vitrification of the mesophase can provide a reason for the upper temperature limit of metastability. This could also explain the large range of small mesophase entities growing out of devitrified RAF seen as 'annealing peaks' in Fig. 12. Once a portion of the RAF of the mesophase with a T_g up to the annealing temperature is devitrified, it can, on cooling, order to a CD glass with a stability governed by

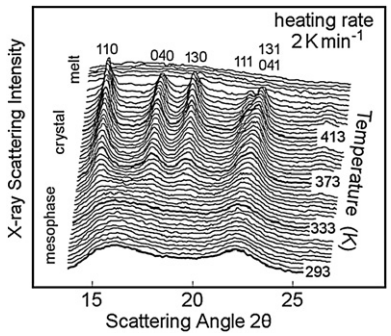

Fig. 21. Temperature-resolved wide-angle X-ray data on heating condis-crystalline iPP at a rate of 2 K min^{-1} [155]. The mesophase at ambient temperature is identified by the two broad peaks, the monoclinic crystals by their characteristic diffraction patterns [1, Fig. IV.5 and 7].

mesophase size and perfection. Ultimately, when annealing at temperatures toward the high temperature end of region I in Fig. 12, even the original mesophase of the 'ref.' curve devitrifies and transforms into the monoclinic crystal. This more stable (metastable) crystal is still not in equilibrium, the distance being fixed by its internal defects, the limited crystallinity, and the coupled RAF. In Fig. 14, the RAF of the monoclinic iPP is similarly devitrified and ordered into mesophase by cold crystallization after quenching. This detailed discussion of the crystallization of iPP stresses the need for many new research directions with better characterized samples, more precise thermal histories, and better structure and calorimetric analyses.

Temperature-resolved WAXS provides evidence that the mesophase orders smoothly to the monoclinic structure on heating in the temperature range II of Fig. 12, beginning when the 2*3/1 helix becomes mobile [94]. Fig. 21 shows a series of WAXS scans during heating of the mesophase of iPP (see also [39, Fig, 4.9]). The mesophase starts to change to monoclinic crystals above 340 K, in good accord with Fig. 12. The halo related to the distance between the parallel aligned chains in the mesophase splits into the 110, 040, and 130 reflections of the monoclinic crystal, and the halo assigned to repeating period, splits into the 111, 131, and 041 reflections of the monoclinic crystal. The melting of the monoclinic crystals is recognized in Fig. 21 by the disappearance of all diffraction peaks and the formation of a residual single broad halo, characteristic of the melt (see also [1, Figs. IV 5 and 7]). Due to different approaches of the data reduction and sample preparation, the exact temperature range of final melting varies [114,128,135,136,145–147], but usually is more than 20 K lower than T_m° (see also Sect. 3.1).

While there exists structure-based information about the direct transition of the iPB mesophase to the crystal without intermediate melting [148–150], similar reports about iPP initially were lacking. Fig. 21, as well as the calorimetry of Fig. 12, indicate that the phase transformation is not connected with global melting. There is no indication of the amorphous scattering in Fig. 21 before ultimate melting, and for Fig. 12, prior melting would require a 15 times bigger endotherm than the transition exotherm. The identification of the mesophase as a CD glass provides a simple mechanism based on the large-amplitude motion.

Additional information about the local nature of the transition can be gained from Fig. 22. It shows AFM images of initially quenched, and subsequently annealed iPP [151]. The nodular habit of the mesophase does not change on transition to the monoclinic phase. While the AFM images of Fig. 22 have been collected at ambient temperature, temperature-resolved AFM data gave similar results [152]. Fig. 23 quantifies the temperature-dependence of the size of the nodules on annealing and clearly illustrates that up to

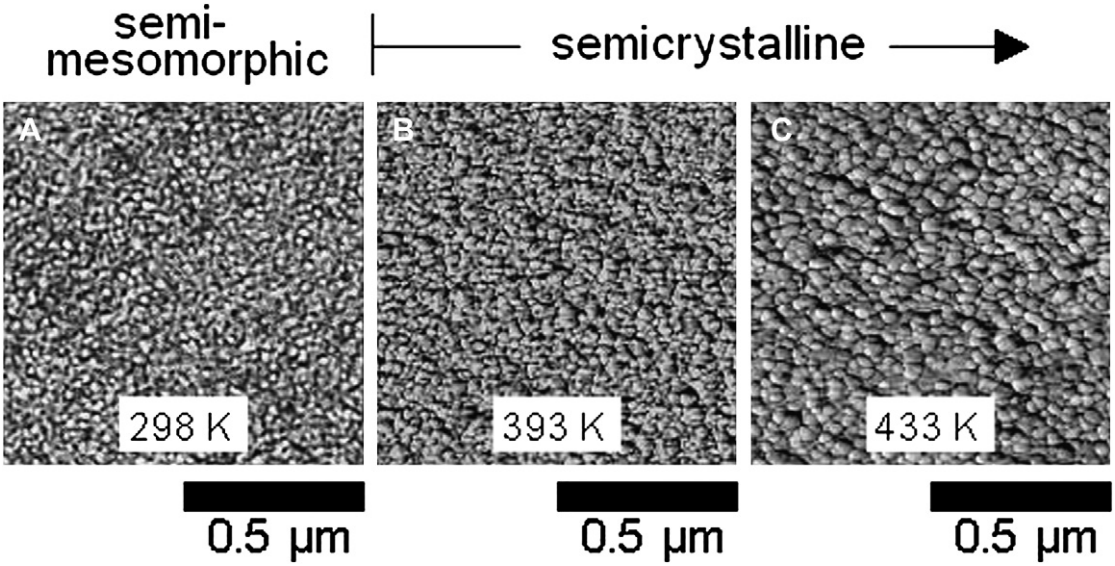

Fig. 22. Three AFM images of initially quenched iPP, collected at ambient temperature after annealing at 298 K (A), 393 K (B), and 433 K (C). Adapted with permission from [151]. Copyright 2008 American Chemical Society.

400 K, heating does not affect the size (and shape) of the ordered domains. The major increases of the crystal dimensions go parallel with the start of the premelting endotherm (region III in Fig. 12). These results are also in general agreement with research using different instrumentation [112,129]. For example, Geil et al. reported that "major change in morphology" is only observed on annealing at temperatures higher than the onset of the α-relaxation at about 393 K [112]. Final proof of melting followed by recrystallization would be the appearance of monoclinic α_2 crystals (see Sect. 3.1).

Major progress regarding the thermal stability of the mesophase has been achieved by FSC [60,63,64]. It is known for many years that fast heating can suppress major perfection of the phases and allows to study the zero entropy production transitions of the structures that become unstable at higher temperature [153]. This well established analysis method relies on sufficiently fast calorimetry to bypass any annealing or recrystallization and is limited only by the possible superheating of the transitions [154].

Further DSC experiments and the extension with FSC is described in Ref. [155] for iPP for samples grown at 300 K with path H1 of Fig. 18. The DSC curves were taken with heating rates from 2 to 100 K min^{-1} and are similar to the traces in Fig. 12 of the mesophase annealed at 285 and 309 K. All DSC curves displayed a first, small endotherm (I) between 310 and 320 K, a small exotherm (II) between 360 and 370 K, and a final, large endotherm (III) at ≈430 K.

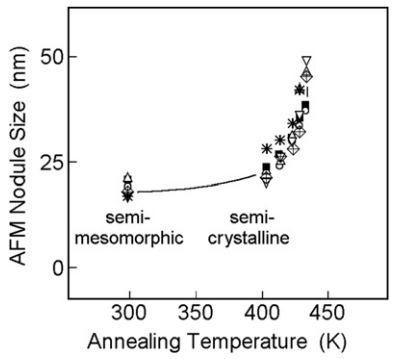

Fig. 23. The AFM nodule size of initially quenched iPP as a function of the temperature of annealing. Annealing at elevated temperature was performed for a period of 60 min. The different symbols represent data obtained on samples quenched at different rates. Adapted from [130]. Copyright 2006, with permission from Elsevier.

Fig. 24 shows the FSC results. Three examples of the measurements with heating rates between 600 and 40,000 K s^{-1} are displayed. They were quenched to the amorphous glass by cooling with a rate of 10,000 K s^{-1} (path C2 of Fig. 18). The amorphous samples were then heated for ordering at 300 K for 30 s, long enough to complete the mesophase formation (see Fig. 17). After renewed quick quenching, the mesophase was analyzed by heat capacity measurement at the heating rates marked in Fig. 24. The three characteristic temperature-ranges of the DSC traces are marked I, II, and III as before in Fig. 12. The exotherms have disappeared, and the large final melting peak has first shifted to lower temperature and decreases sharply in latent heat. Finally, at 40,000 K s^{-1} heating rate, only endotherm I remains, showing the melting peak of the mesophase at ≈360 K, free of reorganization to the monoclinic phase.

The interpretation of the 40,000 K s^{-1} curve in Fig. 24 is straightforward. All CD glass produced at 300 K melts without reorganization in temperature region I at 358 K. At 6000 K s^{-1} this peak moved to 347 K and decreased to 67% (including a small shoulder at 363 K). At 600 K s^{-1}, peak I moved further to 340 K and the area deceased to about 15% (not counting the shoulder). These two and 15 intermediate cooling rates analyzed in [155] show that at lower heating rates the original mesophase glass increasingly transforms on heating to the stable monoclinic crystals (region II in Fig. 12). For the interpretation of the change of the melting peak of the mesophase, its glass transition and that of its RAF need to be separated from the baseline. Both glass transitions are heating rate dependent and could influence the melting.

In summary, the combination of the multiple techniques led to a better understanding of iPP crystallization and melting. The ordering of parts of the molecules affects the properties of the remaining amorphous sections and ultimately precludes further ordering. In iPP, the crystallinity limit is usually 50 ± 20%. One must study mesophase, MAF, and RAF glass transitions and intramolecular helix mobility to assess the metastability of the CD glass. Finally, one has to be able to separate the melting and reorganization to judge crystal size and perfection.

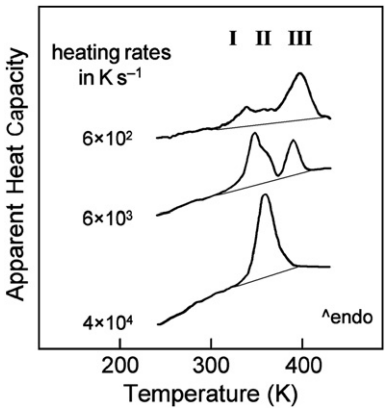

Fig. 24. Apparent heat capacity of semi-mesomorphic iPP as a function of temperature on heating at three different rates by FSC. The mesophase was grown isothermally at 300 K for 30s (see Fig. 18, mode H1, followed by a renewed quenching before analysis at the indicated heating rates). The data were normalized to constant endotherms above the drawn baselines. Adapted with permission from [155]. Copyright 2009 American Chemical Society.

4. The phases of isotactic poly(1-butene) (iPB)

4.1. Polymorphism in iPB

The three main polymorphic forms of isotactic poly(1-butene) (iPB) are called I, II, and III. They correspond to modes of chain packing with different helices, 2*3/1, 2*11/3, and 2*4/1, respectively. Fig. 3 shows the helix repeat for the three iPB helices with the helix axis placed vertically (from bottom to top) in the plane of the paper.

Melt crystallization of iPB yields the tetragonal crystalline lattice of space group $P\bar{4}$, (form II), with a low density of 0.90 g cm^{-3} [156,157]. Each unit cell of the crystal contains two repeats of two 2*11/3 helices with opposite chirality, i.e., 44 molecular repeating units, and a coordination number of four for the helices [156–158]. The helices share no symmetry elements with the unit cell. Form II is kinetically favored when iPB is crystallized by cooling of the unstrained melt at atmospheric pressure, but it is unstable. Upon storage at room temperature, it spontaneously transforms into the twinned trigonal form I. The transformation is completed after about 10 days. It is increasingly metastable at higher or lower temperatures [159,160].

Crystals of the stable form I of iPB contain chains of left-handed and right-handed 2*3/1 helix conformations, packed in a trigonal space group $R\bar{3}c$ with a density of 0.951 g cm^{-3} [160]. The unit cell is drawn in Fig. 11 (as in iPP, the neighboring helices are all drawn isoclined which would reduce the symmetry to $R3c$). Only the average of statistically anticlined helices could satisfy the centers of symmetry and glide planes in Fig. 11. Together, both symmetry elements would require both inclinations on the same helix, an impossible structure. It can result from the X-ray diffraction only if the inclinations vary randomly in position from chain to chain or are located in sufficiently small domains not to be resolved by the analysis. The 3_1 and 3_2 screw axes of the crystal coincide with the helix axes with appropriate chirality, allowing an interpenetration of the neighboring helices with coordination number 3.

The third polymorph, form III, grows from solutions on evaporation of the solvent. It consists of 2*4/1 helices, two of which are packed in an orthorhombic unit cell with space group $P2_12_12_1$ [20,148,161] and a density close to that of form II and an approximately hexagonal close pack of the helices without becoming part of the crystal lattice symmetry [20]. The lower packing density than form I makes the form III also a metastable phase. It converts spontaneously to the form I on drawing.

Two additional crystal structures, named I′ and II′ can be produced by crystallization from the melt under high pressure [162,163]. These two polymorphs are characterized by X-ray diffraction patterns as being similar to forms I and II, respectively, but with broader crystalline reflection peaks [164]. The various crystal structures of iPB can grow or interconvert also under different conditions of preparation. For instance, form I can be obtained by annealing of modifications I′ and III at 363–373 K, as well as on casting from solution. The various preparation methods of the five polymorphs are summarized in [150,162–165].

4.2. Molecular motion within iPB crystals

The small-amplitude vibrations in iPB are not expected to vary significantly between the polymorphs. They were analyzed and linked to the experimental c_p of a semi-crystalline sample of form I [27]. The large-amplitude molecular motion within the polymorphs was studied by NMR (^{1}H relaxation and line shapes, ^{13}C one-dimensional and two-dimensional high-resolution solid state [140,166–168]). At temperatures below T_g of the bulk-amorphous phase, rotation of the methyl group is similar for all ordered polymorphs and the glass. This equivalence arises from the weaker intramolecular interactions in the 2*3/1 helices of form I which compensate much of its denser intermolecular packing than in form II [166]. Forms I, II, and III also show additional side group rotation below T_g. At temperatures above T_g, however, the large-amplitude intramolecular chain motion varies with crystal structure. A detailed characterization of the motional behavior revealed the existence of slow rotational jumps at rates of about 10 s^{-1} in the helices of form III, but only the tetragonal form II shows a degree of motion that allows it to be classified as condis crystal above the T_g of the amorphous iPB [140]. Form I′ of iPB melts at 360–370 K, only the polymer chains in form I are rigid up to ≈360 K.

4.3. Crystallization kinetics of iPB mesophase (form II)

As already stated above, crystallization of iPB from the melt yields the tetragonal mesophase, crystal form II. In contrast to iPP (see Fig. 18), the nucleation of the mesophase of iPB is mostly heterogeneous. By droplet experiments, homogeneous nucleation was observed below 270 K, more than 140 K below T_m° [169]. Overall, four temperature-ranges were identified from the resulting crystal morphology [170]:

1. Below the experimental melting point, there is first the usual temperature gap where the melt is metastable and crystal growth cannot occur (see [1, Sect. 5.1]).
2. From 363 K on, there is a temperature region of about 20 K where a small number of heterogeneous crystal nuclei become active, these nuclei are limited in number and appear sporadically in time, giving rise to large spherulites.
3. At temperatures lower than 343 K, a more intense crystal nucleation takes place, probably due activation of a different, athermal, heterogeneous nucleation, which results in the simultaneous growth of a large number of small, but well-defined, spherulites.
4. At very low temperatures from 270 K to T_g (at 249 K [3]) homogeneous nucleation occurs. An increasingly high number of nuclei grow, so that the nucleated ordered regions impinge at early stages of their growth, ultimately giving rise to a nodular morphology (see Sect. 3.3).

The dependence of linear growth rate of iPB spherulites on temperature was quantified from 313 to 386 K by optical microscopy [170,171]. The growth rate has a maximum at 333 K. A temperature and molar mass dependent change in morphology of the crystals of form II was observed [172–174]. At higher temperatures, single crystals with a quadratic, platelike, hedritic morphology grow [175], while at lower temperatures the common spherulitic superstucture results. Examples of these two morphologies are illustrated with Fig. 25. Crystallization for the same sample conducted at lower temperatures shows increasingly larger numbers of spherulites of smaller size, as expected from a larger number of active heterogeneous nuclei. The change to hedrites in samples of low molar mass (upper micrographs in Fig. 25) occurs at lower temperature than for higher mass (lower right picture of Fig. 25) [174]. At the temperature of prominent hedrite growth, the 2*11/3 helices have already reached a high degree of intramolecular mobility (see Sect. 4.2), so that the lamellar crystals reach better perfection and develop more extended fold lengths [173]. During the transformation from form II to form I the different morphologies are preserved.

It was suggested, that this change in crystallization mechanism of the mesophase occurs when the crystal thickness is similar to the radius of gyration of the chains in the melt, allowing the hedrites to consist of more extended chains [173]. In the light of the long-known properties of condis crystals [5,39] it is more likely that chain extension is enhanced by the increased intramolecular helix mobility at higher temperature than by being governed by the pre-crystallization random coil macroconformation. All extended-chain crystal growth from random coils is connected to condis crystals, as mentioned in Sect. 2.2 for PE.

4.4. Thermal properties of iPB mesophase (crystal form II)

Figs. 26 and 27 show the experimental total specific heat capacity (c_p *Tot*) and the frequency-dependent reversing specific heat capacities (c_p *Rev*) for form II crystals. The data were obtained by temperature-modulated DSC (TMDSC) [2] on samples cooled to the starting temperature of the analysis immediately after isothermal crystallization at 371 K [175]. The c_p *Rev* was measured with three modulation periods (p). The c_p *Tot* reveals a glass transition centered at 245 K, caused by the MAF, followed by a weak and broad exotherm, perhaps due to some form II to I transformation in the room temperature region (see Fig. 27). Next, the experimental c_p *Tot* slowly increases, but remains below the c_p of the liquid iPB until the onset of fusion at ≈370 K. Melting is represented by a large endotherm at low temperature, due to the fusion of form II grown directly from the melt, and a smaller endotherm at higher temperature, revealing fusion of a small amount of form I crystals, converted from form II after crystallization, during the cooling from T_c to 213 K, and during the subsequent heating scan.

The data in Fig. 27 allow to divide the composition of iPB into crystals of form II (condis crystals), MAF, and RAF. The fractional crystallinity is 0.62, the MAF equals 0.19, and the difference of ≈0.18 is taken as an estimate of the RAF. These three phases vary in amount with different crystallization conditions, as exhibited in Figs. 28 and 29. A higher amount of RAF and lower crystallinity is observed for samples ordered at lower temperatures (see Fig. 28) or using faster cooling rates (see Fig. 29). The MAF, in contrast, decreases somewhat when increasing the crystallization temperature, but is

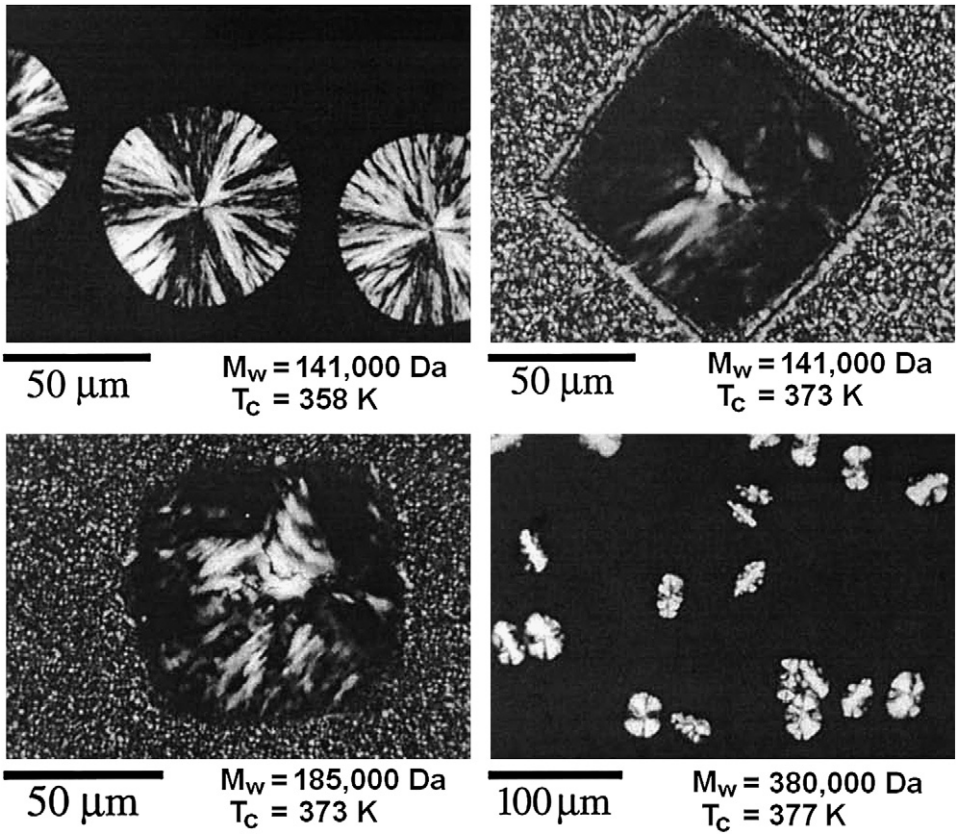

Fig. 25. Optical micrographs documenting the morphology development of iPB of various molar masses, taken between crossed polarizers. The upper left and lower right pictures were taken during the crystallization at T_c. Those at the upper right and lower left were first cooled rapidly from T_c to room temperature in order to obtain images with higher contrast from a background of small spherulites which crystallized at the lower temperature. The quadratic crystals show only little birefringence and show up better within such background of small spherulites grown on cooling. (Reprinted in part with permission from Ref. [173], copyright 2001, American Chemical Society).

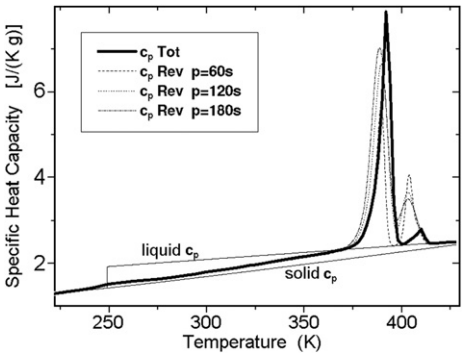

Fig. 26. Specific heat capacity of iPB, crystal form II, after isothermal crystallization at 371 K and subsequent cooling to 213 K. (Reprinted in part with permission from Ref. [175], copyright 2008, Elsevier).

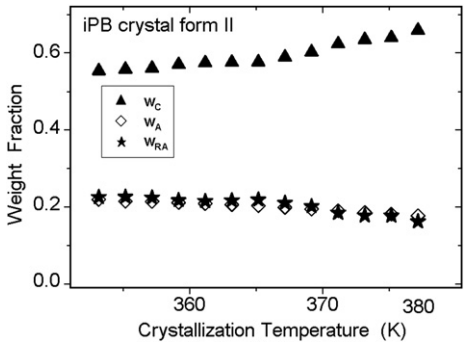

Fig. 28. Crystalline fraction (w_C), MAF (w_A), and RAF (w_{RA}) of form II iPB after isothermal crystallization and subsequent cooling to 213 K, in dependence of the isothermal crystallization temperature (T_c). (Reprinted in part with permission from Ref. [175], copyright 2008, Elsevier).

less affected by changing the cooling rate. These trends support the assignment of the RAF to the form II crystals.

In Fig. 27 the experimental c_p *Tot* and c_p *Rev* by TMDSC are compared to the baselines expected for the different phase compositions. From below the glass transition of the MAF and up to 265 K there is no difference between c_p *Tot* and c_p *Rev*, indicating the relative composition of the sample remains unchanged. This is followed by the above mentioned shallow exotherm, likely due to some form II to I transition. From ≈290 K, c_p *Tot* increases beyond the baseline due to the MAF and at ≈322 K it reaches and crosses the baseline calculated from the two-phase model, interpreted as the RAF having gone through its glass transition. Beyond 322 K the frequency-dependence of the c_p *Rev* plots reveals the occurrence of reversing thermal processes with some exchanges of latent heat (order-disorder processes) [176,177].

This assessment leads to an estimate of the temperature-dependence of the devitrification of the RAF, as illustrated in Fig. 30. The RAF coupled to the condis phase (form II crystals) starts to gradually mobilize about 10 K above the end of the T_g of the MAF, and completes its devitrification at ≈322 K. As shown in Fig. 27, at this temperature the c_p *Rev* curves intersect a two-phase baseline, confirming that above 322 K all amorphous material has a liquid-like c_p. The particular iPB sample of Fig. 30 was isothermally grown at $T_c = 371$ K, far above the temperature of full devitrification of the RAF, i.e., the RAF can develop its glassy character not simultaneously with the growth of the condis crystals, but only on cooling to lower temperature.

The mobility of the condis phase was shown by NMR to begin also at ≈250 K (see Sect. 4.2), but seems to contribute little to the heat capacity below 320 K. It reaches the liquid c_p just before the beginning of major melting of the mesophase at ≈370 K (see Fig. 27). One might thus consider the mesophase to be a CD glass until ≈320 K, but with some residual local chain mobility, perhaps similar to the local, large-amplitude conformational motion in PE. A fully mobile condis crystal, however, has developed only closer to 370 K, the temperature where the hedrite morphology shown in Fig. 25 can develop. On heating, many small and macromolecular condis mesophases have been seen to reach a c_p as known for the liquid phase before the beginning of the isotropization endotherm. (For examples see [2, Figs. 2.68 and 5.143].)

4.5. Transformation of the mesophase to the stable crystal form I

The transformation of iPB from the metastable crystal form II to the stable form I is most important for industrial use since it improves mechanical performance, including higher hardness, stiffness, and strength. The transition occurs without change in morphology, and can be speeded up by deformation and by a number of different nuclei, of which semi-crystalline iPP is specially effective [21,150,178,179]. The transformation begins at nucleation sites within the crystal and requires the transport of new helices within the surrounding crystal [150]. The 2*11/3 helices are locally mobile over the whole range of transformation temperatures (see Sect 4.2), but on addition to the crystal surface of

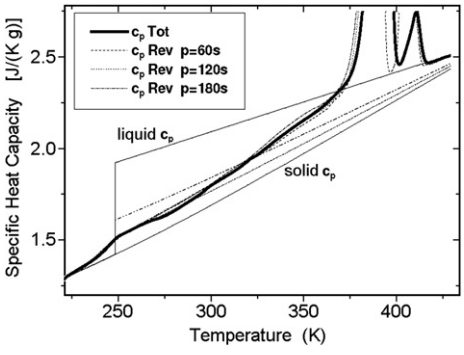

Fig. 27. Enlargement of the curves of Fig. 26 in the area of baseline comparison. The four close to linear baselines correspond from top to bottom to the extrapolated melt (liquid); crystal and MAF (two-phase model); crystal, MAF and RAF (three phase model); and solid. (Reprinted in part with permission from Ref. [175], copyright 2008, Elsevier).

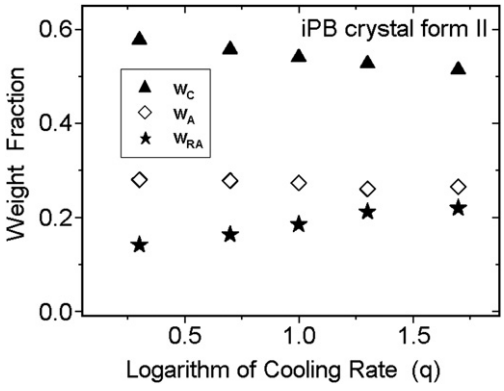

Fig. 29. Crystalline fraction (w_C), MAF (w_A), and RAF (w_{RA}) of form II iPB after non-isothermal crystallization, plotted as a function of the logarithm of cooling rate, q, from the melt in units of K min^{-1} (Reprinted in part with permission from Ref. [175], copyright 2008, Elsevier).

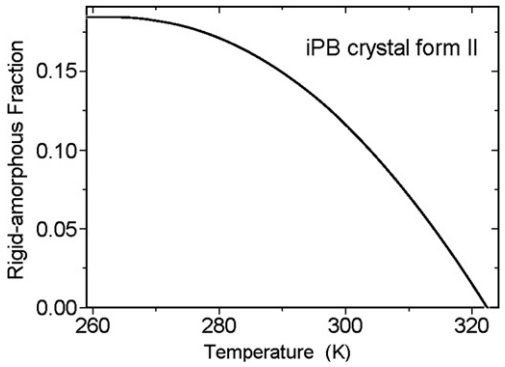

Fig. 30. The RAF (w_{RA}) of the form II crystals of iPB after isothermal crystallization at $T_c = 371$ K and cooling to 213 K as a function of temperature during the subsequent heating at 20 K min^{-1}. (Reprinted in part with permission from Ref. [175], copyright 2008, Elsevier).

form I, they become rigid 2*3/1 helices. The 2*3/1 helix is much more extended as can be seen from Fig. 3 and also it achieves a denser packing in the crystal form I. Once in the rigid 2*3/1 helix, they seem not to be able to reverse the transition to remove remaining defects. These polymorphic transitions are neither accompanied by a change in crystallinity, nor by a change in crystal morphology.

Fig. 31 contains a comparison of DSC traces taken immediately after ordering (to form II) and after storage at room temperature when conversion to crystal form I was completed [180,181]. For the analyzed sample, the melting peak temperature changed from 389 K for the mesophase to 401 K for the stable crystal form. The enthalpy of fusion more than doubled, as has been widely reported in the literature (form II: 3.495 ± 0.2; form I: 7.910 ± 0.6 kJ mol^{-1} [22,181,182]). The RAF is also significantly affected by the transformation. While the crystallinity remains almost unchanged, the RAF increases from 40% to 60% of the total amorphous fractions [180]. Together, these results and the data on structure and molecular motion in Sects. 4.1 and 4.2 prove the crystals of form I to be more stable than form II.

The transition from form II to I changes the temperature-dependence of the thermodynamic functions of the three phases in addition to the RAF to MAF ratio. The glass transition of the MAF in form I is more broadened and the T_g of the RAF moves to higher temperature when compared to form II, as seen in the insert of Fig. 31. In form II, the RAF undergoes its broad glass transition from above T_g of the MAF to ≈322 K, while in form I the glass transition range of the RAF reaches to ≈370 K.

Quasi-isothermal TMDSC allows a more precise analysis of the temperature range from the glass transitions to melting [2]. With this technique, experiments were run with a modulation amplitude of ±0.2 K and a period of 60 s at a set of temperatures, T_o [180]. One set of measurements was made in steps of 5 K for modulation times of 16 min. In the temperature range where c_p *Rev* was not constant at the end of the 16 min experiments, a separate set of was done with a duration of 360 min. In these latter cases the heat capacity can, furthermore, be extrapolated to identify not only c_p *Rev*, but also the reversible c_p.

Fig. 32 illustrates that the reversing melting peak of form I by TMDSC disappears almost completely when analyzing with quasi-isothermal TMDSC. More details of the quasi-isothermal TMDSC can be discerned in the upper graph of Fig. 33. At ≈370 K, the upper limit of the glass transition of its RAF is reached. Within the irreversible melting peak from the standard DSC, the increase of the reversible c_p goes largely parallel with the amount melted when considering the instrument lag in the standard DSC experiment. This observation supports the view that the crystal form I becomes mobile at the time of melting, as one commonly assumes for standard crystals. In the frame of the present discussion of phases as summarized in Fig. 2, this means melting and glass transition of the polymer chain occur simultaneously [50].

The quasi-isothermal TMDSC of the condis crystals (crystal form II), is depicted in the lower graph of Fig. 33. According to the c_p, liquid-like mobility is reached at ≈370 K for the whole sample, amorphous, and mesophase, while for form I crystals this level of mobility coincides with T_m at ≈400 K. As mentioned in Sect. 4.4, it is a frequent observation that mesophases such as condis and liquid crystals of flexible macromolecules and small molecules reach a liquid-like mobility below their begin of melting, i.e., they go through a glass transition below the temperature range of ultimate isotropization [5,39,50]. The upper end of the glass transition of the RAF of form II condis crystals is at 322 K, as seen also in Fig. 27. Some reversible latent heat is indicated in the region where the crystals of form II melt, in line with the frequent observations that the more rigid chains in form I crystals (2*3/1 helices) show

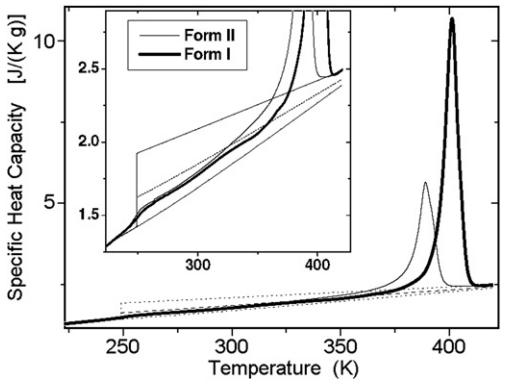

Fig. 31. Specific heat capacity of iPB after crystallization from the melt at 30 K min^{-1}. The thin line refers to iPB analyzed immediately after crystallization to give form II crystals, the thick solid line refers to iPB stored at room temperature after crystallization to convert all crystals to form I. The insert in the upper left is an enlargement of the plots in the baseline c_p area. (Reprinted in part with permission from Ref. [180], copyright 2009, American Chemical Society).

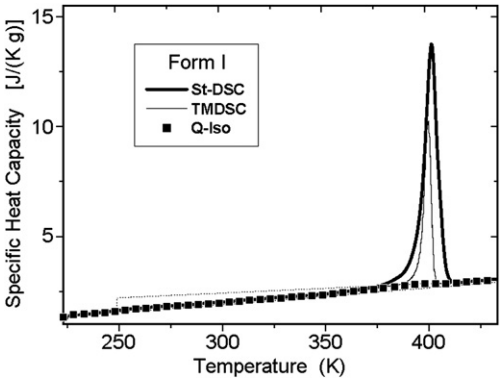

Fig. 32. Specific heat capacity of iPB form I (after crystallization from the melt at 30 K min^{-1} and storage at room temperature). The thick solid line is the total heat capacity by conventional DSC at 20 K min^{-1}, the thin line is the reversing specific heat capacity measured by TMDSC. The solid squares represent the heat capacity at each T_o eliminating all slow processes by measurement with quasi-isothermal TMDSC. (Reprinted in part with permission from Ref. [180], copyright 2009, American Chemical Society).

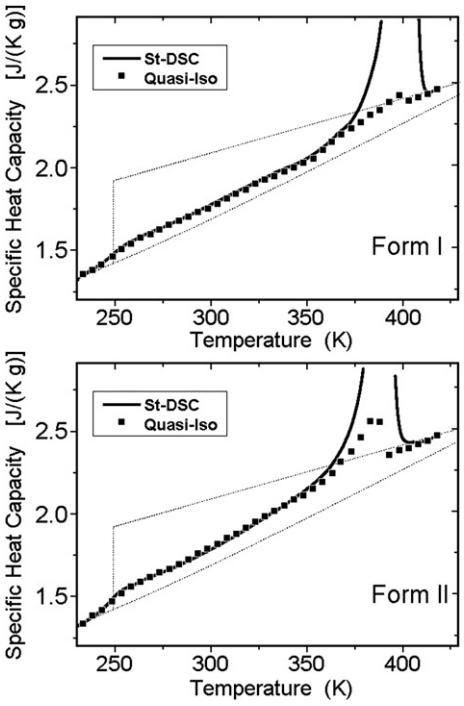

Fig. 33. Specific heat capacity of iPB measured by quasi-isothermal TMDSC. Upper graph: Form I, crystallization from the melt at 0.5 K min^{-1} and storage at room temperature as for Fig. 32. Lower graph: Form II, measured immediately after crystallization from the melt at 0.5 K min^{-1}. (Reprinted in part with permission from Ref. [180], copyright 2009, American Chemical Society).

a smaller amount of locally reversible melting than the form II crystals (2*11/3 helices) [51].

5. Comparison of the mesophases and conclusions

New insight is presented into the properties of the mesophases of the first three members of the alkene polymer family, PE, iPP, and iPB which proved largely different. The analysis was achieved by combining information on intramolecular and intermolecular large-amplitude molecular motion, phase structure, and thermodynamic stability for the various phases that make up their global structures.

The similarities of the three polymers are expressed in the molten state by all three having the same density ($\approx$0.86 g cm^{-3} at room temperature). The equilibrium melting shows a unique variation in T_m° of the crystal structures which are stable at ambient conditions, namely 414, 460, and 411 K for PE, iPP, and iPB with corresponding heats of fusion at T_m° of 8.22, 8.70, and 7.90 J K^{-1} (mol of 2-carbon repeating unit)$^{-1}$. The T_gs mirror the melting temperatures with their bulk-amorphous values of 237, 270, and 249 K, respectively. Overall, these crystal and bulk-amorphous properties give little insight into the different behavior and properties of this important group of industrial polymers.

Major differences among PE, iPP, and iPB arise from their various helix structures as displayed in Fig. 3 and the packing of these on ordering. The intramolecular, large-amplitude chain motion along the chain in form of local gauche-trans conformational rotations develops on heating out of the corresponding low temperature torsional oscillations. In all solid phases of PE, this motion begins already at $\approx$120 K. In amorphous PE, this large-amplitude motion becomes cooperative above $\approx$150 K and causes the typical increase of C_p for the glass transition. In crystalline PE, a similar larger increase begins >250 K is, however, not completed before melting intervenes. For the 2*3/1 helices seen in the stable crystals of iPP and iPB, such motion begins, in contrast, only at $\approx$360 K. The density for PE crystals at room temperature is 1.00 g cm^{-3}, higher than in iPP and iPB crystals (both $\approx$0.95 g cm^{-3}). This density difference is caused by differences in the packing of the helices. The heats of fusion mirror the differences in intermolecular contacts achieved on crystallization when calculated per mole of total C-atoms (in the main-chain and side groups): 4.11, 2.9, and 2.0 kJ mol^{-1}, respectively.

The molecular coupling between crystalline and amorphous phases imparts restrictions on the molecular motion of the surrounding amorphous. For PE, this coupling is least among the three polymers. It causes only a broadening of the glass transition of the surrounding MAF to higher temperature, while for the helical structures of iPP and iPB a considerable amount of RAF is developed. The lesser molecular coupling was observed for PE to be central in creating its ultimate mechanical properties by allowing the creation of a metastable, oriented, noncrystalline phase which extended to greater lengths than the crystals. As in all semi-crystalline polymers, the changes in the amorphous phase limit the crystallinity. Similar differences show up also in the upper limit of the temperatures for homogeneous crystal nucleation. Their distance from the equilibrium T_m increases from a low of 55 K for PE, to 105 K for iPP, and to 140 K for iPB.

Of the three polymers only PE has an equilibrium mesophase, a condis phase at high temperature and pressure. This condis mesophase possesses a largely increased intramolecular conformational mobility. The condis crystals of PE are chain-folded when growing from the melt, as is typical for all flexible, linear macromolecules. The lesser density and greater intramolecular mobility at the higher temperature make PE the only of these three polymers which was shown to subsequently to growth can fully extend the folded-chains. This mobility within the condis crystals, the absence of RAF, and the lesser density-differential between mesophase and the melt also helps to move all surrounding, coupled amorphous molecule-segments into the crystal. Thus, crystallization under pressure can yield extended-chain crystals with close to 100% crystallinity. On release of the hydrostatic pressure and cooling, the mesophase retains its equilibrium morphology and transforms to the orthorhombic, extended-chain crystal structure.

From the melt, the growth of stable, monoclinic iPP crystals slows close to the freezing of the helix mobility, the beginning of homogeneous crystal nucleation, and the T_g of the RAF. At low temperature, iPP orders to a metastable condis glass. This CD glass is similar in helix conformation (2*3/1) and crystallinity to the stable, monoclinic phase. The helix, however, is frequently interrupted by defects. The condis glass converts spontaneously to the monoclinic crystal after it exceeds its own glass transition (estimated to be at 360 K). The transition has a rather small latent heat since its main process involves only the intramolecular correction of the local, non-equilibrium helix defects and a small improvement in crystal symmetry causing an increase of the heat of fusion by $\approx$7%.

The iPB, in contrast to iPP, always forms a mesophase on cooling from the melt (crystal form II). The mesophase contains the more mobile 2*11/3 helices, completely different from the 2*3/1 helices of the stable, trigonal crystals (form I). The 2*3/1 helices are rigid below $\approx$360 K, while the 2*11/3 helices stay internally mobile to 240 K, close to the glass transition of the bulk-amorphous phase. In the upper temperature region of the growth of the mesophase, close to its class transition, there is enough mobility in the 2*11/3 helices to undergo a larger amount of chain extension. The low intermolecular interaction of the 2*11/3 helices cause the mesophase to have a small heat of fusion (3.5 kJ mol^{-1} versus 7.9 kJ mol^{-1} for the stable crystal form I). Thus, the metastable condis state arises out of its possessing a more mobile helix,

a smaller heat of crystallization, and a low density (0.90 g cm^{-3}) which is closer to that of the melt than to crystal form I. It seems likely that short segments the 2*11/3 helix are also present in the melt, and that 2*3/1 helix segments, found in the iPP melt, are not a big part of the iPB melt. The transformation of the mesophase of iPB to the stable crystal is intermolecular instead intramolecular, as was seen for iPP. This means, it undergoes a nucleation step of the new phase with its rigid helix structure and much higher density. The helices of the RAF attached to the form I crystals has an upper limit of T_g of ≈370 K. The rigidity of the iPB 2*3/1 helix and its possible absence in the melt should thus provide the main reasons for the lack of the direct nucleation and growth of the stable crystal form I from the melt.

A detailed study of the three title polymers by the contributing authors and the large amount of information in the literature about these polymers were needed to clarify their vastly different mesophase behaviors. Progress was possible by comparing more contributing factors than commonly assessed and expanding the classical scheme of treatment of phases and their transition as summarized in Fig. 2. It is interesting to note that the more than 150 year old Ostwald's rule of stages is at the root of the solution of the problem of formation of the growth of the mesophases. Their metastability, however, could only be understood when studying their glass transitions and the large-amplitude motion within the polymer chain. It was also noted, that many of the theories of crystal nucleation and growth as well as their defects developed for small molecules must be modified for macromolecules. Extending this improvement in understanding to all flexible, linear macromolecules may lead to the considerable progress needed to further optimize polymeric materials for specific applications.

Acknowledgments

Until 2006, the work at The University of Tennessee at Knoxville and Oak Ridge National Laboratory was supported by the Division of Materials Research, National Science Foundation, Polymers Program, Grant # DMR-9703692 and the Division of Materials Sciences and Engineering, Office of Basic Energy Sciences, U.S. Department of Energy at Oak Ridge National Laboratory, managed and operated by UT-Battelle, LLC, for the U.S. Department of Energy, under contract number DOE-AC05-00OR22725.

The research on isotactic polypropylene presented in this paper has partly been funded by the Deutsche Forschungsgemeinschaft (DFG) (RA and CS) and the European Union (CS).

References

[1] Wunderlich B. Macromolecular physics, vol. 1, crystal structure, morphology, defects; vol. 2, nucleation, crystallization, annealing; vol. 3, crystal melting. New York: Academic Press. 1976, 1980. Electronically searchable PDF reprints with a new preface, published in 2009, are available via (heading: 'Books and more'), and through ATHAS (heading: 'Teaching'), www.scite.eu; 1973, http://athas.prz.rzeszow.pl; 1973.
[2] Wunderlich B. Thermal analysis of polymeric materials. Berlin: Springer, ISBN 978-3-540-23629-0; 2005. Online version, www.springer.com/3-540-23629-5; 2005.
[3] The ATHAS Data Bank of the thermodynamic functions and glass transition temperatures of polymers. It is available from Pyda M, http://athas.prz.rzeszow.pl.
[4] Wunderlich B, Baur H. Heat capacities of linear high polymers. Fortschr Hochpolymeren Forsch (Adv Poly Sci) 1970;7:151–368.
[5] Wunderlich B, Grebowicz J. Thermotropic mesophases and mesophase transitions of linear, flexible macromolecules. Adv Poly Sci 1984;60/61:1–59.
[6] Wunderlich B. Thermodynamic description of condensed phases. In: 37th NATAS conf. on thermal analysis and applications, in Lubbock, TX, Sept. 20–23, Schoch E, editor. CD edition 2009; 37:15 pages. J Thermal Anal Cal 2010, in print.
[7] Wunderlich B. Crystallization during polymerization. Fortschr Hochpolymeren Forsch (Adv Poly Sci) 1968;5:568–619.
[8] Wunderlich B. Effect of decoupling of molecular segments, microscopic stress-transfer, and confinement of the nanophases in semicrystalline polymers. Macromol Rapid Comm 2005;26:1521–31.
[9] Suzuki H, Grebowicz J, Wunderlich B. The glass transition of polyoxymethylene. Br Poly J 1985;17:1–3.
[10] Bamberger E, Tschirner F. Action of diazomethane on β-aromatic hydroxylamines. Ber Deutschen Chem Ges 1900;33:955–9.
[11] Fawcett EW, Gibson RO, Perrin MW, Paton JG, Williams EG. Ethylene polymers. Imperial Chemical Industries Ltd; 1937. Patent, GB 471, 590 19370906.
[12] Hogan JP. Catalysis of the Phillips Petroleum Company polyethylene process. Appl Ind Catal 1983;1:149–76.
[13] Ziegler K, Holzkamp E, Breil H, Martin H. Aluminum in organic chemistry. VII. Polymerization of ethylene and other olefins. Angew Chem 1955;67:426.
[14] Mathot VBF, editor. Calorimetry and thermal analysis of polymers. Munich: Hanser Publishers; 1993.
[15] Andresen A, Cordes HG, Herwig J, Kaminsky W, Merck A, Mottweiler R, et al. Halogen-free soluble Ziegler catalysts for ethylene polymerization. Angew Chem 1976;88:689–90.
[16] Triplett KB. The evolution of Ziegler–Natta catalysts for propylene polymerization. Appl Ind Catal 1983;1:177–205.
[17] Natta G. A new class of polymers from α-olefins having exceptional structural regularity. J Poly Sci 1955;16:143–54.
[18] Sicilia DB. A most invented invention. Invention Technol Magazine 1990;6/1:44–51.
[19] Hogan JP, Banks RL. Solid polymers of olefins. US Patent 1983:4376851, A 19830315.
[20] Cojazzi G, Malta V, Celotti G, Zannetti R. Crystal structure of form III of isotactic poly-1-butene. Macromol Chem 1976;177:915–26.
[21] Azzurri F, Flores A, Alfonso GC, Baltá Calleja FJ. Polymorphism of isotactic poly(1-butene) as revealed by microindentation hardness. 1. Kinetics of the transformation. Macromolecules 2002;35:9069–73.
[22] Silvestre C, Di Lorenzo ML, Di Pace E. Crystallization of polyolefins. In: Vasile C, editor. Handbook of polyolefins. New York: Marcel Dekker, Inc.; 2000. p. 223–48 [Chapter 9].
[23] Belfiore LA, Schilling FC, Tonelli AE, Lovinger AJ, Bovey FA. Magic angle spinning carbon-13 NMR spectroscopy of three crystalline forms of isotactic poly(1-butene). Macromolecules 1984;17:2561–5.
[24] Clark KJ, Turner-Jones A, Sandiford DJH. Polyolefins with unbranched side chains. Chem Ind (London) 1962;47:2010–2.
[25] Qiu W, Sworen J, Pyda M, Nowak-Pyda E, Habenschuss A, Wagener KB, et al. Effect of the precise branching of polyethylene at each 21st CH_2 group on its phase transitions, crystal structure, and morphology. Macromolecules 2006;39:204–17.
[26] Lieser G, Wegner G, Smith JA, Wagener KB. Morphology and packing behavior of model ethylene/propylene copolymers with precise methyl-branch placement. Colloid Poly Sci 2004;282(8):773–81.
[27] Bu HS, Aycock W, Wunderlich B. Heat capacities of solid, branched macromolecules. Polymer 1987;28:1165–76.
[28] Kitaigorodsky AI. Molecular crystals and molecules. New York: Academic Press; 1973. see also Organicheskaja Kristallokhimiya. Moscow: Press of the Acad Sci USSR, 1955. Revised English translation, New York: Consultants Bureau, 1961.
[29] Bunn CW. Crystal structure of long-chain normal paraffin hydrocarbons. "Shape" of the methylene group. Trans Farad Soc 1939;35:482–91.
[30] Turner-Jones A. The triclinic crystal form of polymethylenes and polyethylenes. J Poly Sci 1962;62(174):S53–6.
[31] Seto T, Hara T, Tanaka K. Phase transformation and deformation processes in oriented polyethylene. Jpn J Appl Phys 1968;7(1):31–42.
[32] Wunderlich B. Motion in polyethylene. II. Vibrations in crystalline polyethylene. J Chem Phys 1962;37:207–1216.
[33] Barnes J, Fanconi B. Critical review of vibrational data and force field constants for polyethylene. J Phys Chem Ref Data 1978;7:1309–21.
[34] Wunderlich B. Specific heat of polyethylene single crystals. J Phys Chem 1965;69:2078–81.
[35] Bassett DC, Block S, Piermarini GJ. High pressure phase of polyethylene and chain extended growth. J Appl Phys 1974;45:4146–50.
[36] Wunderlich B, Arakawa T. Polyethylene crystallized from the melt under elevated pressure. J Poly Sci Part A 1964;2:3697–706.
[37] Wunderlich B, Melillo L. Morphology and growth of extended-chain crystals of polyethylene. Makromol Chem 1968;118:250–64.
[38] Yasuniwa M, Enoshita R, Takemura T. X-ray studies of polyethylene under high pressure. Jpn J Appl Phys 1976;15:1421–8.
[39] Wunderlich B, Möller M, Grebowicz J, Baur H. Conformational motion and disorder in low and high molecular mass crystals. Berlin: Springer; 1988 [Adv Poly Sci, Vol. 87].
[40] Sumpter BG, Noid DW, Liang GL, Wunderlich B. Atomistic dynamics of macromolecular crystals. Adv Poly Sci 1994;116:27–72.
[41] Müller A. An X-ray investigation of normal paraffins near their melting points. Proc Roy Soc London Ser A 1932;138:514–30.
[42] Broadhurst MG. Analysis of the solid-phase behavior of the normal paraffins. J Research Natl Bur Stand Sect A 1962;66:241–9.
[43] Asahi T. The hexagonal phase and melt of low-molecular-weight polyethylene. J Poly Sci Poly Phys 1984;22:175–82.
[44] Wunderlich B. Motion in polyethylene. III. The amorphous polymer. J Chem Phys 1962;37:2429–32.

[45] Gaur U, Wunderlich B. The glass transition temperature of polyethylene. Macromolecules 1980;13:445–6.
[46] Jin Y, Wunderlich B. The heat capacity of *n*-paraffins and polyethylene. J Phys Chem 1991;95:9000–7.
[47] Kim Y, Strauss HL, Snyder RG. Conformational disorder in crystalline *n*-alkanes prior to melting. J Phys Chem 1989;93(21):7520–6.
[48] Qiu W, Habenschuss A, Wunderlich B. The phase structures of nylon 6.6 as studied by temperature-modulated calorimetry and their link to X-ray structure and molecular motion. Polymer 2007;48:1641–50.
[49] Qiu W, Pyda M, Nowak-Pyda E, Habenschuss A, Wunderlich B. Reversible melting and crystallization of high molar mass poly(oxyethylene) measured by temperature-modulated DSC and X-ray diffraction. J Poly Sci Part B Poly Phys 2007;45:475–89.
[50] Wunderlich B. The glass transition as key to identify solid phases. J Appl Poly Sci 2007;105:49–59.
[51] Wunderlich B. Reversible crystallization and the rigid-amorphous phase in semicrystalline macromolecules. Prog Poly Sci 2003;28/3:383–450.
[52] Kunz M, Möller M, Heinrich U-R, Cantow H-J. Electron spectroscopic imaging studies on polyethylene, chain-folded and extended-chain crystals. Makromol Chem Symp 1988;20/21:147–58.
[53] Cheng J, Fone M, Reddy VN, Schwartz KB, Fisher HP, Wunderlich B. Identification and quantitative analysis of the intermediate phase in a linear high density polyethylene. J Poly Sci Part B Poly Phys 1994;32:2683–93.
[54] Litvinov VM, Mathot VBF. Partitioning of main and side-chain units between different phases: a solid-state ^{13}C NMR inversion-recovery cross-polarization study on a homogeneous, metallocene-based, ethylene-1-octene copolymer. Solid State Nucl Mag Res 2002;22:218–34.
[55] Kwon YK, Boller A, Pyda M, Wunderlich B. Melting and heat capacity of gel-spun, ultra-high-molar-mass polyethylene fibers. Polymer 2000;41:6237–49.
[56] Fu Y, Chen W, Pyda M, Londono D, Annis B, Boller A, et al. Structure-property analysis for gel-spun, ultrahigh molecular mass polyethylene fibers. J Macromol Sci Phys 1996;B35:37–87.
[57] Chen W, Fu Y, Wunderlich B, Cheng J. The Morphology of gel-spun polyethylene fibers investigated by solid state ^{13}C NMR. J Poly Sci Part B Poly Phys 1994;32:2661–6.
[58] Wunderlich B, Cormier CM. Seeding of supercooled polyethylene with extended chain crystals. J Phys Chem 1966;70:1844–9.
[59] Cormia RL, Price FP, Turnbull D. Kinetics of crystal nucleation in polyethylene. J Chem Phys 1962;37:1333–40.
[60] Minakov AA, Schick C. Ultrafast thermal processing and nanocalorimetry at heating and cooling rates up to 1 MK/s. Rev Sci Inst 2007;78:073902-1–073902-10.
[61] Zhuravlev E, Schick C. Fast scanning power compensated differential scanning nano-calorimeter: 2. Heat capacity analysis. Thermochim Acta 2010;505:14–21.
[62] Zhuravlev E, Schick C. Fast scanning power compensated differential scanning nano-calorimeter: 1. The device. Thermochim Acta 2010;505:1–13.
[63] Adamovsky SA, Minakov AA, Schick C. Scanning microcalorimetry at high cooling rate. Thermochim Acta 2003;403:55–63.
[64] Adamovsky SA, Schick C. Ultra-fast isothermal calorimetry using thin film sensors. Thermochim Acta 2004;415:1–7.
[65] Breedon Jones J, Barenberg S, Geil PH. Amorphous linear polyethylene. Polymer 1979;20:903–16.
[66] Gezovich DM, Geil PH. Morphology of quenched polypropylene. Poly Eng Sci 1968;8:202–9.
[67] Addink EJ, Beintema J. Polymorphism of crystalline polypropylene. Polymer 1961;2:185–93.
[68] Turner-Jones A, Aizlewood JM, Beckett DR. Crystalline forms of isotactic polypropylene. Makromol Chem 1964;75:134–58.
[69] Natta G, Corradini P. Structure and properties of isotactic polypropylene. Nuovo Cim 1960;15(Suppl):40–51.
[70] Mencik Z. Crystal structure of polypropylene. Chemicky Prumysl 1960;10:377–81. See also J Macromol Sci, Phys 1972;6:101–115.
[71] Guerra G, Petraccone V, Corradini P, De Rosa C, Napolitano R, Pirozzi B, et al. Crystalline order and melting behavior of isotactic polypropylene (α form). J Poly Sci Poly Phys 1984;22:1029–39.
[72] Auriemma F, Ruiz de Ballesteros O, De Rosa C, Corradini P. Structural disorder in the α form of isotactic polypropylene. Macromolecules 2000;33:8764–74.
[73] Padden Jr FJ, Keith HD. Crystallization in thin films of isotactic polypropylene. J Appl Phys 1966;37:4013–20.
[74] Binsbergen FL, De Lange BGM. Morphology of polypropylene crystallized from the melt. Polymer 1968;1:23–40.
[75] Lotz B, Wittmann JC, Lovinger AJ. Structure and morphology of poly (propylenes): a molecular analysis. Polymer 1996;37:4979–92.
[76] Padden Jr FJ, Keith HD. Spherulitic crystallization in polypropylene. J Appl Phys 1959;30:1479–84.
[77] Keith HD, Padden Jr FJ, Walter NM, Wyckoff HW. Evidence for a second crystal form of polypropylene. J Appl Phys 1959;30:1485–8.
[78] Meille SV, Ferro DR, Brückner S, Lovinger AJ, Padden FJ. Structure of β-isotactic polypropylene: a long-standing structural puzzle. Macromolecules 1994;27:2615–22.
[79] Lotz B, Kopp S, Dorset D. Original crystal structure of polymers with ternary helixes. Comptes Rendus de l'Academie des Sci Serie IIb 1994;319:187–92.
[80] Leugering HJ. Effect of crystal structure and superstructure on some properties of polypropylene. Makromol Chem 1967;109:204–16.
[81] Aboulfaraj M, G'Sell C, Ulrich B, Dahoun A. In situ observation of the plastic deformation of polypropylene spherulites under uniaxial tension and simple shear in the scanning electron microscope. Polymer 1995;36:731–42.
[82] Kotek J, Raab M, Baldrian J, Grellmann W. The effect of specific β-nucleation on morphology and mechanical behavior of isotactic polypropylene. J Appl Poly Sci 2002;85:1174–84.
[83] Sauer JA, Pae KD. Structure and thermal behavior of pressure-crystallized polypropylene. J Appl Phys 1968;39:4959–68.
[84] Turner-Jones A. Development of the γ-crystal form in random copolymers of propylene and their analysis by DSC and X-ray methods. Polymer 1971;12:487–508.
[85] Brückner S, Meille SV. Non-parallel chains in crystalline γ-isotactic polypropylene. Nature 1989;340:455–7.
[86] Meille SV, Brückner S, Porzio W. γ-Isotactic polypropylene. A structure with non-parallel chain axes. Macromolecules 1990;23:4114–21.
[87] Hosier IL, Alamo RG, Esteso P, Isasi JR, Mandelkern L. Formation of the α and γ polymorphs in random metallocene – propylene copolymers. Effect of concentration and type of comonomer. Macromolecules 2003;36:5623–36.
[88] De Rosa C, Auriemma F, Ruiz de Ballesteros O, Resconi L, Camurati I. Crystallization behavior of isotactic propylene – ethylene and propylene – butene copolymers: effect of comonomers versus stereodefects on crystallization properties of isotactic polypropylene. Macromolecules 2007;40:6600–16.
[89] Natta G, Peraldo M, Corradini P. Smectic mesomorphic form of isotactic polypropylene. Rend Accad Naz Lincei 1959;26:14–7.
[90] Natta G. Progress in the stereospecific polymerization. Makromol Chem 1960;35:94–131.
[91] Grebowicz J, Lau S-F, Wunderlich B. The thermal properties of polypropylene. J Poly Sci Symp 1984;71:19–37.
[92] Bu HS, Cheng SZD, Wunderlich B. Addendum to the thermal properties of polypropylene. Makromol Chem Rapid Commun 1988;9:75–7.
[93] Wu ZQ, Dann VL, Cheng SZD, Wunderlich B. Fast DSC applied to the crystallization of polypropylene. J Thermal Anal 1988;34:105–14.
[94] Schaefer D, Spiess HW, Suter UW, Fleming WW. Two-dimensional solid-state NMR studies of ultraslow chain motion: glass transition in atactic poly (propylene) versus helical jumps in isotactic poly(propylene). Macromolecules 1990;23:3431–9.
[95] Poddubnyi VI, Lavrent'ev VK, Shevelev VA, Mikhailova NV, Sidorovich AV, Baranov VG. Melt crystallization of polypropylene: structure formation. Poly Bull 1984;11:41–7.
[96] Jin Y, Hiltner A, Baer E, Masirek R, Piorkowska E, Galeski A. Formation and transformation of smectic polypropylene nanodroplets. J Polym Sci Part B Polym Phys 2006;44:1795–803.
[97] Ibarretxe Uriguen J, Bremer L, Mathot VBF, Groeninckx G. Preparation of water-borne dispersions of polyolefins: new systems for the study of homogeneous nucleation of polymers. Polymer 2004;45:5961–8.
[98] Chen W, Wunderlich B. Nanophase separation of small and large molecules. Macromol Chem Phys 1999;200:283–311.
[99] Wunderlich B. Thermodynamics and properties of nanophases. Thermochim Acta 2009;49(2):2–15.
[100] Piccarolo S. Morphological changes in isotactic polypropylene as a function of cooling rate. J Macromol Sci Phys 1992;B31:501–11.
[101] Brucato V, Piccarolo S, Titomanlio G. Crystallization kinetics in relation to polymer processing. Makromol Chem Macromol Symp 1993;68:245–55.
[102] Piccarolo S, Alessi S, Brucato V, Titomanlio G. Crystallization behavior at high cooling rates of two polypropylenes. In: Dosiere M, editor. Crystallization of polymers. Dordrecht: Kluwer; 1993. p. 475–80.
[103] Brucato V, Piccarolo S, La Carubba V. An experimental methodology to study polymer crystallization under processing conditions. The influence of high cooling rates. Chem Eng Sci 2002;57:4129–43.
[104] Gradys A, Sajkiewicz P, Minakov AA, Adamovsky S, Schick C, Hashimoto T, et al. Crystallization of polypropylene at various cooling rates. Mat Sci Eng 2005;A413/414:442–6.
[105] De Santis F, Adamovsky S, Titomanlio G, Schick C. Scanning nanocalorimetry at high cooling rate of isotactic polypropylene. Macromolecules 2006;39:2562–7.
[106] Silvestre C, Cimmino S, Duraccio D, Schick C. Isothermal crystallization of isotactic poly(propylene) studied by superfast calorimetry. Macromol Rapid Comm 2007;28:875–81.
[107] De Santis F, Adamovsky S, Titomanlio G, Schick C. Isothermal nanocalorimetry of isotactic polypropylene. Macromolecules 2007;40:9026–31.
[108] Burns JR, Turnbull D. Kinetics of crystal nucleation in molten isotactic polypropylene. J Appl Phys 1966;37:4021–6.
[109] Pyda M, Nowak-Pyda E, Heeg J, Huth H, Minakov AA, Di Lorenzo ML, et al. Melting and crystallization of poly(butylene terephthalate) by temperature-modulated and superfast calorimetry. J Polym Sci Part B Polym Phys 2006;44:1364–77.
[110] Turnbull D, Fisher JC. Rate of nucleation in condensed systems. J Chem Phys 1949;17:71–3.
[111] Wunderlich B. The influence of liquid to solid transitions on the changes of macromolecular phases from disorder to order. (Based on a lecture given at the 11th Lähnwitz Seminar in Rostock-Warnemünde, June 6–11, 2010). Thermochim Acta, in press.

[112] Hsu CC, Geil PH, Miyaji H, Asai K. Structure and properties of polypropylene crystallized from the glassy state. J Poly Sci Poly Phys 1986;24:2379–401.
[113] Miller RL. On the existence of near-range order in isotactic polypropylenes. Polymer 1960;1:135–43.
[114] McAllister PB, Carter TJ, Hinde RM. Structure of the quenched form of polypropylene. J Poly Sci Poly Phys 1978;16:49–57.
[115] Ashby GE, Hoeg DF. Concerning the measurement of isotacticity in propylene polymers. J Poly Sci 1959;39(Letter, Issue 135):535–9.
[116] Gailey JA, Ralston RH. The quenched state of polypropylene. SPE Trans; 1964:29–33.
[117] Farrow G. Measurement of the smectic content in undrawn polypropylene filaments. J Appl Poly Sci 1965;9:1227–32.
[118] Bodor G, Grell M, Kallo A. Untersuchung des Zustandes von Polypropylen – Vorschlag zur Bestimmung der Kristallinität des Polypropylens. Faserforschung und Textiltechnik 1964;15:527–32.
[119] Corradini P, Petraccone V, De Rosa C, Guerra G. On the structure of the quenched mesomorphic phase of isotactic polypropylene. Macromolecules 1986;19:2699–703.
[120] Corradini P, De Rosa C, Guerra G, Petraccone V. Comments on the possibility that the mesomorphic form of isotactic polypropylene is composed of small crystals of the β crystalline form. Poly Comm 1989;30:281–5.
[121] Auriemma F, De Rosa C, Corradini P. Solid mesophases in semicrystalline polymers: structural analysis by diffraction techniques. Adv Poly Sci 2005; 181:1–74.
[122] Hsu CC, Geil PH, Miyaji H, Asai K. Structure and properties of polybutylene crystallized from the glassy state. J Macromol Sci Phys 1983;B22:489–96.
[123] Yeh GSY, Geil PH. Crystallization of polyethylene terephthalate from the glassy state. J Macromol Sci Phys 1967;B1:235–49.
[124] Meyer M, Van der Sande J, Uhlmann DR. On the structure of glassy polymers. VI. Electron microscopy of polycarbonate, poly(ethylene terephthalate), poly (vinyl chloride), and polystyrene. J Poly Sci Poly Phys 1978;16:2005–14.
[125] Kanig G. Application of the short-time staining for the electron microscopic investigation of the crystallization of polyethylene. Colloid Polym Sci 1983;261:373–4.
[126] Caldas V, Brown GR, Nohr RS, MacDonald JG, Raboin LE. The structure of the mesomorphic phase of quenched isotactic polypropylene. Polymer 1994;35: 899–907.
[127] Ogawa T, Miyaji M, Asai K. Nodular structure of polypropylene. J Phys Soc Jpn 1985;54:3668–70.
[128] Wang ZG, Hsiao BS, Srinivas S, Brown GM, Tsou AH, Cheng SZD, et al. Phase transformation in quenched mesomorphic isotactic polypropylene. Polymer 2001;42:7561–6.
[129] Grubb DT, Yoon DY. Morphology of quenched and annealed isotactic polypropylene. Poly Comm 1986;27:84–8.
[130] Zia Q, Androsch R, Radusch HJ, Piccarolo S. Morphology, reorganization and stability of mesomorphic nanocrystals in isotactic polypropylene. Polymer 2006;47:8163–72.
[131] Zia Q, Androsch R, Radusch HJ, Ingolič E. Crystal morphology of rapidly cooled isotactic polypropylene: a comparative study by TEM and AFM. Poly Bull 2008;60:791–8.
[132] Zia Q, Androsch R. Effect of atomic force microscope tip geometry on the evaluation of the crystal size of semicrystalline polymers. Meas Sci Technol 2009;20:097003 (4pp).
[133] Hayashi H, Hamada F, Suehiro S, Masaki N, Ogawa T, Miyaji H. The 6 m point-focusing small-angle X-ray scattering camera at the high-intensity X-ray laboratory of Kyoto University. J Appl Cryst 1988;21:330–9.
[134] Konishi T, Nishida K, Kanaya T, Kaji K. Effect of isotacticity on formation of mesomorphic phase of isotactic polypropylene. Macromolecules 2005;38: 8749–54.
[135] Konishi T, Nishida K, Kanaya T. Crystallization of isotactic polypropylene from prequenched mesomorphic phase. Macromolecules 2006;39: 8035–40.
[136] O'Kane WJ, Young RJ, Ryan AJ, Bras W, Derbyshire GE, Mant GR. Simultaneous SAXS/WAXS and DSC analysis of the melting and recrystallization behaviour of quenched polypropylene. Polymer 1994;35:1352–8.
[137] Miyamoto Y, Fukao K, Yoshida T, Tsurutani N, Miyaji H. Structure formation of isotactic polypropylene from the glass. J Phys Soc Jpn 2000;69:1735–40.
[138] Mileva D, Zia Q, Androsch R, Radusch HJ, Piccarolo S. Mesophase formation in poly(propylene- *ran*-1-butene) by rapid cooling. Polymer 2009;50:5482–9.
[139] Xu Z, Mays J, Chen X, Hadjichristidis N, Schilling FC, Bair HE, et al. Molecular characterization of poly (2-methyl-1,3-pentadiene) and its hydrogenated derivative, atactic polypropylene. Macromolecules 1985;18:2560–6.
[140] Maring D, Wilhelm M, Spiess HW, Meurer B, Weill G. Dynamics in the crystalline polymorphic forms I and II and form III of isotactic poly-1-butene. J Poly Sci Part B Poly Phys 2000;38:2611–24.
[141] Cao J, Sbarski I. Determination of the enthalpy of solid phase transition for isotactic polypropylene using a modified DSC technique. Polymer 2006;47: 27–31.
[142] van Santen RA. The ostwald step rule. J Phys Chem 1984;88:5768–9.
[143] Wurm A, Ismail M, Kretzschmar B, Pospiech D, Schick C. Retarded crystallization in polyamide-layered silicates nanocomposites caused by an immobilized interphase. Macromolecules 2010;43:1480–7.
[144] Iijima M, Strobl G. Isothermal crystallization and melting of isotactic polypropylene analyzed by time- and temperature-dependent small-angle X-ray scattering experiments. Macromolecules 2000;33:5204–14.
[145] Zannetti R, Celotti G, Fichera A, Francesconi R. The structural effects of annealing time and temperature on the paracrystal-crystal transition in isotactic polypropylene. Makromol Chem 1969;128:137–42.
[146] Martorana A, Piccarolo S, Sapoundjeva D. SAXS/WAXS study of the annealing process in quenched samples of isotactic poly(propylene). Macromol Chem Phys 1999;200:531–40.
[147] Natale R, Russo R, Vittoria V. Crystallinity of isotactic polypropylene films annealed from the quenched state. J Mat Sci 1992;27:4350–4.
[148] Holland VF, Miller RL. Isotactic polybutene-1 single crystals: morphology. J Appl Phys 1964;35:3241–8.
[149] Kopp S, Wittmann JC, Lotz B. Phase II to phase I crystal transformation in polybutene-1 single crystals: a reinvestigation. J Mat Sci 1994;29:6159–66.
[150] Tosaka M, Kamijo T, Tsuji M, Kohjiya S, Ogawa T, Isoda S, et al. High--resolution transmission electron microscopy of crystal transformation in solution-grown lamellae of isotactic polybutene-1. Macromolecules 2000; 33:9666–72.
[151] Zia Q, Mileva D, Androsch R. The rigid amorphous fraction in isotactic polypropylene. Macromolecules 2008;41:8095–102.
[152] Androsch R. In situ atomic force microscopy of the mesomorphic–monoclinic phase transition in isotactic polypropylene. Macromolecules 2008;41:531–3.
[153] Wunderlich B. The melting of defect polymer crystals. Polymer 1964;5: 611–24.
[154] Hellmuth E, Wunderlich B. Superheating of linear high-polymer polyethylene crystals. J Appl Phys 1965;36:3039–44.
[155] Mileva D, Androsch R, Zhuravlev E, Schick C. The temperature of melting of the mesophase of isotactic polypropylene. Macromolecules 2009;42: 7275–8.
[156] Starkweather Jr HW, Jones GA. The heat of fusion of polybutene-1. J Poly Sci Part B Poly Phys 1986;24:1509–14.
[157] Turner-Jones A. Poly-l-butylene type II crystalline form. J Poly Sci Part B Poly Lett 1963;1:455–6.
[158] Turner-Jones A. Cocrystallization in copolymers of α-olefins II—Butene-1 copolymers and polybutene type II/I crystal phase transition. Polymer 1966;7:23–59.
[159] Natta G, Corradini P, Bassi IW. Crystal structure of isotactic poly(1-butene). Nuovo Cimento 1960;15:52–67.
[160] Azzurri F, Gómez MA, Alfonso GC, Ellis G, Marco C. Time-resolved SAXS/WAXS studies of the polymorphic transformation of 1-butene/ethylene copolymers. J Macromol Sci Part B Phys 2004;B43:177–89.
[161] Chau KW, Geil PH. Solution history effects in polybutene-1. J Macromol Sci Phys 1984;23:115–42.
[162] Armeniades CD, Baer E. Effect of pressure on the polymorphism of melt crystallized polybutene-1. J Macromol Sci Phys 1967;1:309–34.
[163] Nakafuku C, Miyaki T. Effect of pressure on the melting and crystallization behaviour of isotactic polybutene-1. Polymer 1983;24:141–8.
[164] Boor Jr J, Youngman EA. Polymorphism in poly-1-butene: apparent direct formation of modification I. J Poly Sci Part B Poly Lett 1964;2:903–7.
[165] Luciani L, Seppälä J, Löfgren B. Poly-1-butene: its preparation, properties and challenges. Progr Poly Sci 1988;13:37–62.
[166] Maring D, Meurer B, Weill G. ^{1}H NMR studies of molecular relaxations of poly-1-butene. J Poly Sci Part B Poly Phys 1995;33:1235–47.
[167] Beckham HW, Schmidt-Rohr K, Spiess HW. Conformational disorder and its dynamics within the crystalline phase of the form II polymorph of isotactic poly(l-butene). ACS Symp Ser 1995;598:242–53.
[168] Miyoshi T, Hayashi S, Imashiro F, Kaito A. Side-chain conformation and dynamics for the form II polymorph of isotactic poly(1-butene) investigated by high-resolution solid-state ^{13}C NMR spectroscopy. Macromolecules 2002;35:6060–3.
[169] Burns JR, Turnbull D. Nucleation of crystallization in molten isotactic poly-1-butene. J Poly Sci Poly Phys 1968;6:775–82.
[170] Silvestre C, Cimmino S, Di Lorenzo ML. Crystallization of Poly(1-butene)/-hydrogenated oligocyclopentadiene blends. J Appl Poly Sci 1999;71: 1677–90.
[171] Monasse B, Haudin JM. Morphologies and regimes of growth of polybutene crystals in phase II. Makromol Chem Makromol Symp 1988;20/21: 295–302.
[172] Cimmino S, Di Lorenzo ML, Silvestre C. Thermal and morphological analysis of isotactic poly(1-butene)/hydrogenated oligocyclopentadiene blends. Thermochim Acta 1998;321:99–109.
[173] Fu Q, Heck B, Strobl G, Thomann YA. Temperature- and molar mass-dependent change in the crystallization mechanism of poly(1-butene): transition from chain-folded to chain-extended crystallization? Macromolecules 2001;34:2502–11.
[174] Acierno S, Grizzuti N, Winter HH. Effects of molecular weight on the isothermal crystallization of poly(1-butene). Macromolecules 2002;35: 5043–8.
[175] Di Lorenzo ML, Righetti MC. The three-phase structure of isotactic poly (1-butene). Polymer 2008;49:1323–31.
[176] Schick C, Wurm A, Mohammed A. Formation and disappearance of the rigid amorphous fraction in semicrystalline polymers revealed from frequency dependent heat capacity. Thermochim Acta 2003;396:119–32.
[177] Di Lorenzo ML, Wunderlich B. Melting of polymers by non-isothermal, temperature-modulated calorimetry: analysis of various irreversible latent heat contributions to the reversing heat capacity. Thermochim Acta 2003;405:255–68.

[178] Azzurri F, Flores A, Alfonso GC, Sics I, Hsiao BS, Baltá-Calleja FJ. Polymorphism of isotactic polybutene-1 as revealed by microindentation hardness. Part II: correlations to microstructure. Polymer 2003;44:1641–5.
[179] Zhang Xia, Zhang Xu, Shi G. The effect of some additives on the form II to form I phase transformation in polybutene-1. Thermochim Acta 1992;205:245–52.
[180] Di Lorenzo ML, Righetti MC, Wunderlich B. Influence of crystal polymorphism on the three-phase structure and on the thermal properties of isotactic poly(1-butene). Macromolecules 2009;42:9312–20.
[181] Chau KW, Yang YC, Geil PH. Tetragonal to twinned hexagonal crystal phase transformation in polybutene-1. J Mater Sci 1986;21:3002–14.
[182] Alfonso GC, Azzurri F, Castellano M. Analysis of calorimetric curves detected during the polymorphic transformation of isotactic polybutene-1. J Thermal Anal Cal 2001;66:197–207.

René Androsch is Privatdozent at the Center of Engineering Sciences at the Martin-Luther-University Halle-Wittenberg (Germany) where he teaches courses in General Materials Science and Polymeric Materials. He studied Polymeric Materials Science at the Technische Hochschule Leuna-Merseburg (Germany), and received his PhD degree in 1993 for research in the field of crystallization of polyester blends. In 1995, René Androsch was awarded with the prestigious Alexander-von-Humboldt Fellowship. Following several research sabbaticals in the groups of John Blackwell in 1996 (CWRU) and Bernhard Wunderlich in 1998/1999 (UTK/ORNL), he completed his Habilitation at the Martin-Luther-University Halle-Wittenberg in 2005. Research interests include structure and morphology of semi-crystalline polymers, polymer crystallization and melting, the polymorphism of polymers, and structure-property relationships.

Maria Laura Di Lorenzo is since 2001 a Research Scientist at the Institute of Chemistry and Technology of Polymers of the Italian National Research Council (ICTP-CNR, Italy). In 1998 she was a Research Associate at the University of Tennessee at Knoxville and the Oak Ridge National Laboratory (USA). Her main research interests focus on the thermal analysis of homopolymers and multi-component polymeric materials. Major investigations concern structure-property relationships, transition kinetics (crystallization, melting, glass transition), morphology, mechanical, and barrier properties. Dr. Di Lorenzo is Head of the Laboratory of Thermal Analysis at ICTP-CNR. She is the author and co-author of 2 patents, and more than 60 articles published in international journals and books. Dr. Di Lorenzo received the "First AIM Award for Young Researchers", from the Italian Association of Science and Technology of Macromolecules (AIM) in 2007 and the "A. Lucci Award", from the Italian Association of Calorimetry and Thermal Analysis (AICAT), for "her innovative contribution to the development of calorimetric and thermoanalytical instruments for the caracterization of polymer-based materials" in 2002.

Christoph Schick is Professor and Head of the Polymer Physics Group at the Institute of Physics of the University of Rostock since 1992. Since 2010 he holds the position of vice dean of the Faculty of Mathematics and Natural Science. He studied Polymer Physics at the Technische Hochschule Leuna-Merseburg (Germany) and received his PhD degree in 1980 for research in the field of glass transition with Prof. E. Donth as his mentor. As a postdoctoral research associate he became interested in the interplay between glass transition and crystallization in polymers. In this field he completed his Habilitation in 1988. Since then, his research focuses on advanced calorimetry as represented by temperature-modulated and fast to ultra-fast scanning methods, applied to polymers, metals, and other substances. He is interested in crystallization, nucleation, and glass transition in these materials. Christoph Schick received the Mettler Toledo Award of the North American Thermal Analysis Society in 2006, The James J. Christensen Memorial Award in Recognition of Outstanding Contributions to the Innovative Development and Use of Calorimetric Equipment of the Calorimetry Conference, USA, in 2008, and in 2010 in Italy, The AICAT-SETARAM Award in recognition of outstanding contributions to advances in the physical knowledge and generation of tools related to ordering, crystallization, aggregation or organization of synthetic polymers.

Bernhard Wunderlich retired in 2001 from the position of Distinguished Scientist and Professor of Chemistry at The University of Tennessee in Knoxville and Oak Ridge National Laboratory which he held since 1988, but still keeps an interest in research and teaching. He had immigrated in 1954 to the US and received his Ph.D. at Northwestern University in Evanston, Illinois in 1957 with Prof. Malcolm Dole as his mentor, he worked in the field of thermodynamics and calorimertry of linear macromolecules. His research interests developed into the solid state of polymers and thermal analysis. In this field he held positions at Northwestern University (1957–1958), Cornell University (1958–1963), Rensselaer Polytechnic Institute (1963–88). Two extended sabbaticals abroad were at the University of Mainz (1967/68) and the Universities of Freiburg and Ulm (1986/87). During his professional career more than 575 technical papers have been published with the help of his 144 students and postdoctoral coworkers. Most important of the 10 books he authored are the three-volume treatise on "Macromolecular Physics" (Academic Press, New York, 1974–80), a textbook on "Thermal Analysis of Polymeric Materials" (Springer, Berlin, 2005), and most recently an autobiography "A Science Career Against all Odds" (Springer, Berlin, 2010). Professor Wunderlich received the Mettler Award in Thermal Analysis and was named one of the outstanding educators of the United States in 1971, was given a Fellowship by the Japanese Society for the Promotion of Science (1983), the Humboldt Award (1986), the Prize for Applied Chemical Thermodynamics of the Swiss Society for Thermoanalytic and Calorimetry (1993), the TA-Instruments Award of the International Confederation of Thermal Analysis and Calorimetry (1996), and the Distinguished Service Award of the North American Thermal Analysis Society (2002). His lifetime achievements were honored at the 2006 NATAS Meeting. In 2007, his three-semester sequence of 36 computer-based lectures on "Thermal Analysis of Materials" became available via the Internet (*www.scite.eu* or *http://athas.prz.rzeszow.pl*).